JCB Journal of Cell Biology

ARTICLE

SNAP23 deficiency causes severe brain dysplasia through the loss of radial glial cell polarity

Masataka Kunii[1,2], Yuria Noguchi[1], Shin-ichiro Yoshimura[1], Satoshi Kanda[1], Tomohiko Iwano[3], Erda Avriyanti[1,4], Nur Atik[1,5], Takashi Sato[6], Ken Sato[2], Masaharu Ogawa[7], and Akihiro Harada[1,2]

In the developing brain, the polarity of neural progenitor cells, termed radial glial cells (RGCs), is important for neurogenesis. Intercellular adhesions, termed apical junctional complexes (AJCs), at the apical surface between RGCs are necessary for cell polarization. However, the mechanism by which AJCs are established remains unclear. Here, we show that a SNARE complex composed of SNAP23, VAMP8, and Syntaxin1B has crucial roles in AJC formation and RGC polarization. Central nervous system (CNS)–specific ablation of SNAP23 (NcKO) results in mice with severe hypoplasia of the neocortex and no hippocampus or cerebellum. In the developing NcKO brain, RGCs lose their polarity following the disruption of AJCs and exhibit reduced proliferation, increased differentiation, and increased apoptosis. SNAP23 and its partner SNAREs, VAMP8 and Syntaxin1B, are important for the localization of an AJC protein, N-cadherin, to the apical plasma membrane of RGCs. Altogether, SNARE-mediated localization of N-cadherin is essential for AJC formation and RGC polarization during brain development.

Introduction

During the development of the mammalian brain, many types of neurons and glial cells are generated from radial glial cells (RGCs) and migrate to their appropriate positions to form the brain structure (Butts et al., 2014; Gupta et al., 2002; Nadarajah and Parnavelas, 2002). RGCs are highly polarized along their apico-basal axis. This polarity contributes to RGC proliferation and differentiation as well as to the migration of postmitotic neurons (Götz and Huttner, 2005). The polarity of RGCs is established and maintained by intercellular adhesions, termed apical junctional complexes (AJCs; Lehtinen and Walsh, 2011; Taverna et al., 2014). The disruption of AJCs is associated with the pathogenesis of several disorders in the human brain, such as hydrocephalus and intraventricular hemorrhage (McAllister et al., 2017; Rodríguez et al., 2012). Thus, AJCs have important roles in the normal development of the mammalian brain.

A number of protein complexes, such as cadherin–catenin complexes, Par–atypical PKC (aPKC) complexes, and Crumbs (Crb)–Patj–Pals1 complexes, are required for the organization of AJCs (Singh and Solecki, 2015; Uzquiano et al., 2018). In particular, the localization of N-cadherin to the apical plasma membrane (PM) is important for the formation of cadherin–catenin complexes that initiate AJC formation (Chenn et al., 1998; Gumbiner, 2005; Miyamoto et al., 2015). The localization of cadherins is regulated by intracellular protein transport machinery (Bryant and Stow, 2004; Cadwell et al., 2016). A number of proteins, such as a Notch regulator, Numb, and a Scribble complex protein, Lgl1, are involved in an endocytic or recycling pathway of N-cadherin in RGCs (Jossin et al., 2017; Rasin et al., 2007); however, it remains unclear how newly synthesized or recycled N-cadherin is properly localized to the apical PM of RGCs.

In polarized cells, such as RGCs, newly synthesized membrane proteins are transported to distinct parts (apical or basolateral) of the cell surfaces by polarized transport machinery (Mellman and Nelson, 2008; Weisz and Rodriguez-Boulan, 2009). Transport vesicles containing membrane proteins fuse with the PM via the facilitation of SNARE proteins. Vesicle-associated membrane protein (VAMP) on the transport vesicles, and Syntaxin (Stx) and synaptosomal-associated protein (SNAP) on the PM form a ternary complex that fuses the membranes (Hong, 2005; Jahn and Scheller, 2006; Südhof and Rothman, 2009). In the central nervous system (CNS), the VAMP2–Stx1A–SNAP25 complex is a well-characterized neuronal SNARE complex that is involved in the fusion of synaptic

---

[1]Department of Cell Biology, Graduate School of Medicine, Osaka University, Osaka, Japan; [2]Laboratory of Molecular Traffic, Department of Molecular and Cellular Biology, Institute for Molecular and Cellular Regulation, Gunma University, Gunma, Japan; [3]Department of Anatomy and Cell Biology, Graduate School of Medicine, University of Yamanashi, Yamanashi, Japan; [4]Department of Dermatology and Venereology, Faculty of Medicine, Padjadjaran University, Bandung, Indonesia; [5]Department of Biomedical Sciences, Faculty of Medicine, Padjadjaran University, Bandung, Indonesia; [6]Laboratory of Developmental Biology and Metabolism, Department of Molecular Medicine, Institute for Molecular and Cellular Regulation, Gunma University, Gunma, Japan; [7]RIKEN Brain Science Institute, Saitama, Japan.

Correspondence to Akihiro Harada: aharada@acb.med.osaka-u.ac.jp; Masataka Kunii: mstk921@acb.med.osaka-u.ac.jp.

© 2020 Kunii et al. This article is distributed under the terms of an Attribution–Noncommercial–Share Alike–No Mirror Sites license for the first six months after the publication date (see http://www.rupress.org/terms/). After six months it is available under a Creative Commons License (Attribution–Noncommercial–Share Alike 4.0 International license, as described at https://creativecommons.org/licenses/by-nc-sa/4.0/).

vesicles with presynaptic PMs (Pevsner et al., 1994; Sutton et al., 1998). Knockout mice deficient in any of the proteins in this complex show impairments in neurotransmission, but they exhibit no abnormalities in brain morphology or AJC formation (Fujiwara et al., 2006; Schoch et al., 2001; Washbourne et al., 2002). Thus, additional SNARE complexes are likely involved in these processes.

Here, we report that SNAP23 plays a crucial role in the localization of N-cadherin to the apical PM of RGCs. SNAP23 is a ubiquitously expressed SNARE protein that belongs to the SNAP25 family and is involved in exocytotic events in diverse cell types (Kunii et al., 2016; Ravichandran et al., 1996; Ren et al., 2015). SNAP23 participates in the transport of glutamate receptors to the postsynaptic region in mature neurons (Suh et al., 2010), but the function of SNAP23 in brain development remains unknown. In this study, we generated CNS-specific SNAP23 knockout (NcKO) mice. NcKO mice exhibited severe hypoplasia of the cerebral cortex and lacked a hippocampus and cerebellum. In the developing brain of NcKO mice, the disruption of AJCs caused the loss of RGC polarity, which resulted in abnormal proliferation and differentiation of RGCs, as well as the death of postmitotic neurons. Using primary cultures of RGCs, we found that SNAP23 is important for the localization of N-cadherin to the PM. Additionally, other SNARE proteins, VAMP8 and Stx1B, interact with SNAP23 to promote the localization of N-cadherin to the apical PM of RGCs. Based on these findings, we conclude that a SNARE complex composed of SNAP23, VAMP8, and Stx1B mediates the localization of N-cadherin to the apical PM and is crucial for the polarization of RGCs in the developing brain.

Results

NcKO mice result in severe hypoplasia of the cerebral cortex and lack of a hippocampus and cerebellum

To elucidate the function of SNAP23 in the developing brain, NcKO mice were generated by crossing *Snap23*$^{f/f}$ mice (Kunii et al., 2016) with Nestin-Cre mice, which drives Cre-mediated recombination in RGCs (Tronche et al., 1999). The NcKO mice were born at a typical Mendelian ratio but died within 3 wk of birth. Perinatal (P0) NcKO mice exhibited internal hemorrhaging in the hindbrain region (Fig. 1 A, arrowhead). 2-wk-old NcKO mice showed growth retardation, severe spatial disorientation, and an ataxic gait (Video 1). At P14, the NcKO brains showed severe hypoplasia of the cerebral cortex, and there was no cerebellum (Fig. 1 B, arrow and arrowhead). The morphological abnormalities of the NcKO brain were already evident at embryonic stages. On embryonic day (E) 16.5, the cerebral cortex (Fig. 1 C, asterisks) and hippocampus (Fig. 1 C, arrows) of the NcKO mice were reduced, and intraventricular hemorrhage was observed in the third ventricle (Fig. 1 C, arrowhead). In the caudal region, there was no middle part of the midbrain (Fig. 1 D, arrowheads) or cerebellar vermis (Fig. 1, D and E, arrows). At P0, the NcKO brains exhibited additional severe malformations. The size of the cerebral cortex was drastically reduced, and the neuronal layers were disorganized (Fig. 1 F, asterisks). The hippocampus was completely absent (Fig. 1 F, arrows). In contrast, the medial cortex and diencephalon were relatively unaffected, but the third ventricles were enlarged (Fig. 1 F, arrowheads). In the caudal region, most of the midbrain and cerebellum were lost, and the aqueduct of the midbrain and the fourth ventricle were markedly enlarged (Fig. 1, G and H, asterisks).

To assess morphological abnormalities during development, we observed earlier-stage embryos. Immunoblotting showed that the expression of SNAP23 in the NcKO brain was retained at E12.5 but was greatly reduced at E13.5 (Fig. 1 I). Consistent with these results, the cerebral cortex and cerebellum were still intact at E12.5 in the NcKO mice; however, at E13.5, the smooth surfaces of the ventricular walls were disorganized (Fig. 1, J and K, arrows). SNAP23 was expressed in both RGCs and neurons in the control cortex at E13.5. In RGCs, SNAP23 was localized to both the apical and basal processes, but favored the apical side (Fig. S1, A and B, arrows). In contrast, SNAP25 was expressed mainly in postmitotic neurons (Fig. S1 B). SNAP23 was not expressed in the E13.5 NcKO brain, confirming the sufficient expression of Cre recombinase at this stage (Fig. 1, L and M). Thus, SNAP23 is essential for the normal development of the cerebral cortex and cerebellum.

RGCs in NcKO mice lose their apico-basal polarity and exhibit abnormal interkinetic nuclear migration (INM)

In the E13.5 WT brain, RGCs extend short apical processes to the ventricular surface and long basal processes to the pial surface from the soma localized in the ventricular zone (VZ; Miyata et al., 2001; Noctor et al., 2001). The nucleus and soma migrate up and down the VZ in a cell cycle–dependent manner—this process is referred to as INM (Miyata et al., 2015). We addressed whether the depletion of SNAP23 would influence apico-basal polarization and INM. In the control cortex, apical and basal processes positive for Nestin, the intermediate filaments specifically expressed in RGCs, normally extend radially through the cortex. In contrast, the processes in the NcKO cerebral cortex were shortened or absent, and a number of round-shaped cells were observed (Fig. 2 A). When the cerebral cortices were stained with a Pericentrin antibody, a marker of the basal body of primary cilium, the basal bodies were located just beneath the lateral ventricular surface of the control cortex; however, they localized diffusely throughout the VZ of the NcKO cortex (Fig. 2 B, arrows). These observations suggest the misorientation of RGCs in the NcKO mice. Additionally, staining for Pax6, a marker of neural progenitor cells, including RGCs, revealed a significant decrease in the number of progenitors in the NcKO cortex (Fig. 2, C and D). Similar to that in the cerebral cortex, a loss of RGC polarity was observed in the NcKO cerebellum (Fig. 2, E and F). The number of Pax6-positive granule cell progenitors in the rhombic lip area was markedly decreased in the NcKO cerebellum (Fig. 2, G and H).

Mitotic RGCs were labeled with BrdU or a phospho-histone H3 (PH3) antibody to investigate cell cycle–dependent INM. In the control cortex, the nuclei of S-phase cells, which exhibited BrdU incorporation, were in the upper region (pial side) of the VZ. In contrast, S-phase cells in the NcKO cortex exhibited a more apical (ventricle side) localization (Fig. 2, I and J). Moreover,

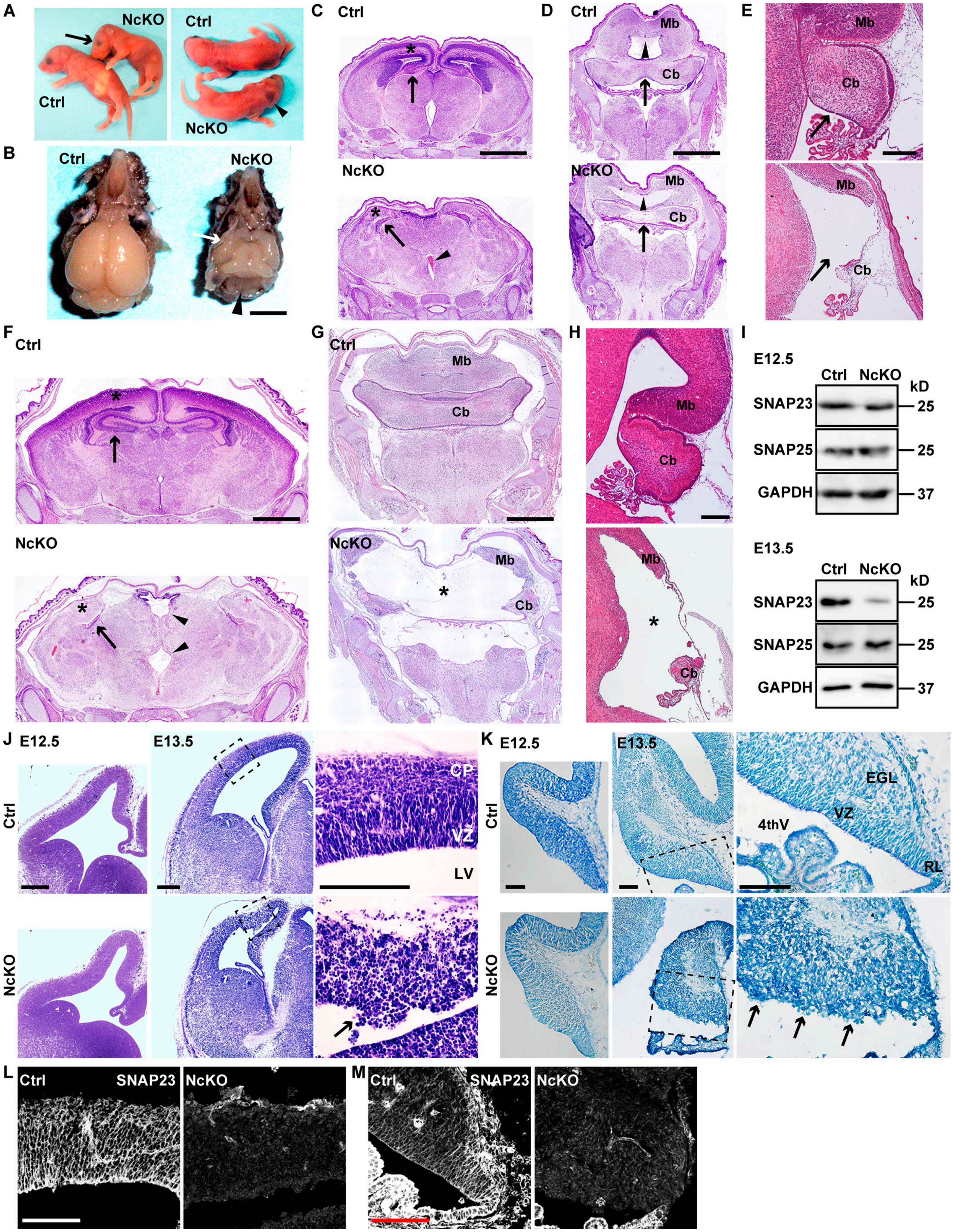
A
NcKO
Ctrl
Ctrl
NcKO
B
Ctrl
NcKO
C
Ctrl
NcKO
*
D
Ctrl
Mb
Cb
NcKO
Mb
Cb
E
Mb
Cb
Mb
Cb
F
Ctrl
NcKO
*
G
Ctrl
Mb
Cb
NcKO
Mb
*
Cb
H
Mb
Cb
Mb
*
Cb
I
E12.5
Ctrl
NcKO
kD
SNAP23
25
SNAP25
25
GAPDH
37
E13.5
Ctrl
NcKO
kD
SNAP23
25
SNAP25
25
GAPDH
37
J
E12.5
E13.5
Ctrl
NcKO
CP
VZ
LV
K
E12.5
E13.5
Ctrl
NcKO
EGL
VZ
4thV
RL
L
Ctrl
SNAP23
NcKO
M
Ctrl
SNAP23
NcKO

Figure 1. **NcKO mice show severe hypoplasia of the cerebral cortex and have no hippocampus or cerebellum. (A)** The appearance of control (Ctrl) and NcKO mice at P0. NcKO mice exhibited small eyes (arrow) and internal hemorrhaging (arrowhead). **(B)** Representative brains of the P14 Ctrl and NcKO mice. The NcKO brain shows hypoplasia of the cerebral cortex (arrow) and has no cerebellum (arrowhead). Scale bar, 5 mm. **(C–H)** Hematoxylin-eosin staining of coronal sections in the middle (C and F) and caudal region (D and G) and sagittal sections of the cerebellum (E and H) at E16.5 (C–E) and P0 (F–H). Asterisks, arrows, and arrowheads in C and F indicate the cerebral cortex, hippocampus, and third ventricle, respectively. Arrows and arrowheads in D and E indicate the vermis of the cerebellum (Cb) and middle part of the midbrain (Mb), respectively. Asterisks in G and H indicate the enlarged aqueduct of the midbrain and the fourth ventricle, respectively. Scale bars, 1 mm. **(I)** Immunoblots showing SNAP23 and SNAP25 in the brain. GAPDH blotting was used as a loading control. **(J and K)** Nissl staining in coronal sections of the cerebrum and sagittal sections of the cerebellum at E12.5 and E13.5. Arrows indicate the disorganization of the ventricular walls. Scale bars, 200 µm (J), 100 µm (K). **(L and M)** Expression of SNAP23 in E13.5 brain sections. Scale bars, 50 µm. 4th V, fourth ventricle; CP, cortical plate; EGL, external granular layer; LV, lateral ventricle; RL, rhombic lip; VZ, ventricular zone.

the majority of M-phase cells, which were labeled with PH3, was located at the ventricular surface in the control cortex. However, PH3-positive cells were scattered throughout the NcKO cortex (Fig. 2, K and L). Based on these data, we concluded that SNAP23 plays a significant role in the apico-basal polarization of RGCs and is required for normal proliferation and INM of RGCs.

The NcKO brain exhibits enhanced differentiation, defective migration, and increased apoptosis of newborn neurons

As the apico-basal polarity of RGCs is also necessary for their differentiation into neurons (Götz and Huttner, 2005; Lehtinen and Walsh, 2011; Taverna et al., 2014), we analyzed neurons in the NcKO brain. In the control cerebral cortex, Tuj1- or Tbr1-positive neurons were located at the cortical plate. In contrast, in the NcKO cortex, neurons were also observed in the VZ and the sub-VZ, suggesting migration defects (Fig. 3, A–C). Moreover, the number of neurons was increased in the NcKO cortex (Fig. 3 D). In the NcKO cerebellum, Tuj1-positive neurons were also ectopically located in the VZ (Fig. 3 E, arrows). The numbers of calbindin-positive Purkinje cells and Tbr1-positive cerebellar nuclei neurons were also increased in the NcKO cerebellum (Fig. 3, F–H, arrows). Thus, neural differentiation might be promoted in the NcKO brain. To confirm this, we performed a cell cycle exit analysis. We counted the number of cells that exited the cell cycle 24 h after BrdU incorporation, and the proportion of cells ($BrdU^+$, $Ki67^-$/total $BrdU^+$) was significantly increased in the NcKO cortex and cerebellum (Fig. 3, I–L, arrows). These data suggest that, although the NcKO brain ultimately shows hypoplasia, premature neurogenesis is promoted at the early stage of brain development.

As most of the cerebral cortex and cerebellum is lost in the postnatal NcKO brain, the increasing number of neurons cannot settle in neuronal layers. To address this, we observed apoptosis by staining for cleaved Caspase-3. In the NcKO cerebral cortex and cerebellum, the number of apoptotic cells was clearly increased (Fig. 3, M–O, arrows). Double staining for TUNEL and Pax6 or Tbr1 showed that most TUNEL-positive cells were stained with Tbr1, but not Pax6, suggesting that the apoptotic cells were not RGCs but were neurons (Fig. 3, P and Q, arrows). Thus, increased neuronal cell death seems to be the cause of the reduced brain size in the NcKO mice.

Loss of SNAP23 disrupts the AJCs at the ventricular surface of the RGCs

The formation of AJCs is required to establish and maintain the polarity of RGCs. Protein complexes, such as cadherin–catenin, Par–aPKC, and Crb–PatJ–Pals1 complexes, are involved in the formation of AJCs (Singh and Solecki, 2015; Uzquiano et al., 2018). The phenotype of the NcKO mice is similar to that of mice lacking a component of the AJC, such as N-cadherin, β-catenin, aPKC, Crb2, or Pals1 (Dudok et al., 2016; Imai et al., 2006; Kadowaki et al., 2007; Kim et al., 2010; Machon et al., 2003). Therefore, we investigated the localization of proteins that compose AJCs in the NcKO brain. Sections of the cerebrum and cerebellum were stained with different AJC markers, including N-cadherin, β-catenin, Par3, ZO-1, Crb3, and Pals1. As expected, the expression of all of these markers was substantially decreased or lost at the ventricular surface in the NcKO cerebral cortex and cerebellum, suggesting that the AJCs in the NcKO brain were disorganized (Fig. 4, A–L, arrows). Electron-dense AJCs were rarely observed at the apical region of RGCs in the NcKO cerebral cortex, suggesting a reduction in the size and/or number of AJCs (Fig. 4 M, arrowheads). Based on these results, we conclude that the loss of SNAP23 reduces the number of AJCs, which results in the loss of RGC polarity.

SNAP23 participates in the localization of N-cadherin to the apical PM

SNAP23 is involved in membrane fusion between transport vesicles and the PM in various tissues (Kunii et al., 2016; Ren et al., 2015; Suh et al., 2010). Thus, we hypothesized that SNAP23 might play a role in promoting the localization of AJC proteins to the PM. To confirm this hypothesis, we compared the localization of SNAP23 to N-cadherin or Crb in the WT RGCs. SNAP23 colocalized with N-cadherin in the apical processes of the RGCs (Fig. S1 C). In contrast, Crb3 and its associated protein, Pals1, were localized more apically than SNAP23 (Fig. S1, D and E). Accordingly, SNAP23 might be involved in the localization of N-cadherin to the apical PM. We cultured RGCs isolated from the E13.5 cerebral cortex and depleted SNAP23 with an siRNA to clarify the function of SNAP23 in the intracellular transport of N-cadherin. Control RGCs grew in clumps, and most of the N-cadherin was located at cell boundaries. However, SNAP23-depleted RGCs appeared to be dissociated to a greater extent, and the amount of N-cadherin localized at the PM was decreased (Fig. 5 A). Using an antibody recognizing the ectodomain of N-cadherin, N-cadherin was rarely detected at the PM in the SNAP23-depleted RGCs (Fig. 5 B). Furthermore, a cell surface biotinylation assay showed a marked reduction in the amount of biotinylated N-cadherin at the cell surface of the SNAP23-depleted RGCs (Fig. 5, C and D). Next, we performed cell aggregation assays to determine the strength of RGC adhesion. The

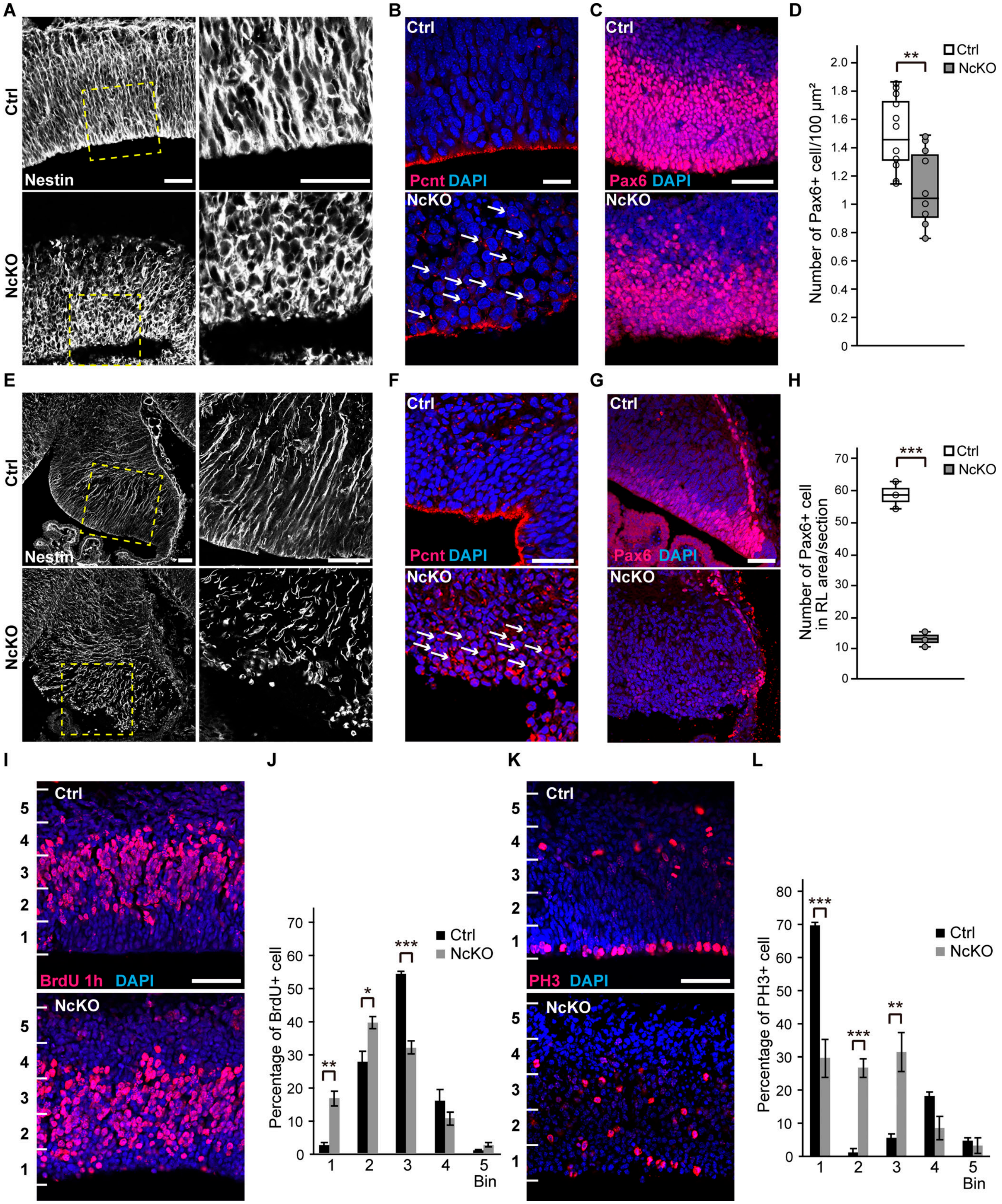
A
Ctrl
NcKO
Nestin
B
Ctrl
Pcnt DAPI
NcKO
C
Ctrl
Pax6 DAPI
NcKO
D
Number of Pax6+ cell/100 μm²
2.0
1.8
1.6
1.4
1.2
1
0.8
0.6
0.4
0.2
0
**
Ctrl
NcKO
E
Ctrl
NcKO
Nestin
F
Ctrl
Pcnt DAPI
NcKO
G
Ctrl
Pax6 DAPI
NcKO
H
Number of Pax6+ cell in RL area/section
70
60
50
40
30
20
10
0
***
Ctrl
NcKO
I
Ctrl
BrdU 1h DAPI
NcKO
5
4
3
2
1
J
Percentage of BrdU+ cell
70
60
50
40
30
20
10
0
**
*
***
Ctrl
NcKO
1
2
3
4
5
Bin
K
Ctrl
PH3 DAPI
NcKO
5
4
3
2
1
L
Percentage of PH3+ cell
80
70
60
50
40
30
20
10
0
***
***
**
Ctrl
NcKO
1
2
3
4
5
Bin

Figure 2. **NcKO RGCs lose their apico-basal polarity. (A)** Nestin stained in coronal sections of the cerebrum at E13.5. Right panels show magnified images of the boxes surrounded by dashed lines in the left panels. Scale bars, 50 µm. **(B)** Pericentrin (Pcnt; red) and DAPI (blue) stained in coronal sections of the cerebrum at E13.5. Arrows indicate abnormal localization of basal bodies in RGCs. Scale bar, 20 µm. **(C)** Pax6 (red) and DAPI (blue) stained in coronal sections of the cerebrum at E13.5. Scale bar, 50 µm. **(D)** Density of the Pax6-positive cells in the E13.5 cerebral cortex (*n* = 12 sections from three mice of each genotype). **(E)** Nestin stained in sagittal sections of the cerebellum at E13.5. Right panels show magnified images of the boxes surrounded by dashed lines in the left panels. Scale bars, 50 µm. **(F)** Pericentrin (red) and DAPI (blue) stained in sagittal sections of the cerebellum at E13.5. Arrows indicate the abnormal localization of the

basal bodies in RGCs. Scale bar, 20 µm. **(G)** Pax6 (red) and DAPI (blue) stained in sagittal sections of the cerebellum at E13.5. Scale bar, 50 µm. **(H)** Number of Pax6-positive cells in the rhombic lip (RL) area in cerebellar sections (*n* = 3 sections from three mice per genotype). **(I)** BrdU (red) and DAPI (blue) stained in coronal sections of the cerebrum at E13.5. Scale bar, 50 µm. **(J)** Distributions of BrdU-positive S-phase RGCs in cerebral sections (*n* = 5 sections from three mice per genotype). **(K)** PH3 (red) and DAPI (blue) stained in coronal sections of the cerebrum at E13.5. Scale bar, 50 µm. **(L)** Distributions of PH3-positive M-phase RGCs in cerebral sections (*n* = 5 sections from three mice per genotype). The box plots represent the maximum and minimum values. The centerlines of the box plots represent the medians of the data. The bar graphs represent the means ± SEM. Significance was calculated by using two-tailed paired Student's *t* tests. Statistical significance is indicated by *P < 0.05, **P < 0.01, or ***P < 0.001. Ctrl, control.

---

number and size of the SNAP23-depleted RGC aggregates were clearly decreased (Fig. S2, A–C). These data suggest that the depletion of SNAP23 in RGCs results in a decrease in the localization of N-cadherin at the PM and cell adhesion.

In our cell surface biotinylation study, the PM localization of other membrane proteins, such as β1-integrin and Ephrin-B1, was also decreased in the SNAP23-depleted RGCs (Fig. 5, C and D). In contrast, the localization of low-density lipoprotein receptor (LDLR) and Na^+/K^+-ATPase was comparable in the control and SNAP23-depleted RGCs, suggesting the cargo selectivity of SNAP23 (Fig. 5, C and D). To confirm whether the decreased localization of N-cadherin to the PM is a major cause of severe malformation, we performed a rescue experiment using in utero electroporation (IUE). The transmembrane domain (TMD) and the cytoplasmic region in cargo proteins are necessary for their sorting in polarized transport (Mellman and Nelson, 2008). We therefore constructed a chimeric protein in which the TMD and part of the cytoplasmic region between the TMD and the p120-catenin binding region of N-cadherin were replaced with the TMD and the cytoplasmic region of LDLR, referred to as N-cadherin–LDLR (Fig. 5 E). We electroporated the N-cadherin–mCherry or N-cadherin–LDLR–mCherry plasmid and Cas9 with the SNAP23 single-guide RNA (sgRNA) plasmid into the cerebral cortex at E13.5. Two days after electroporation of the control plasmid (empty pX330), apical staining of ZO-1 was intact (Fig. 5 F). The staining of ZO-1 was similarly unaffected in the nonelectroporated region (Fig. S4 A). After electroporation of SNAP23 sgRNA and N-cadherin–mCherry, apical ZO-1 staining became less intense and more irregular, suggesting that AJCs were disrupted; furthermore, the boundary of the ventricular surface became irregular in the depleted regions (Fig. 5 F, right panels), which closely resembled the NcKO brain. This result indicated that the disruption of AJCs by SNAP23 depletion was not rescued by the expression of N-cadherin, because it might not have been delivered to the PM. In contrast, apical staining of ZO-1 was observed in the RGCs in which N-cadherin–LDLR–mCherry was expressed (Fig. 5 G, arrowheads) and the ventricular surface became relatively smooth. This finding suggests that this chimeric protein was transported to the PM and formed AJCs even in the absence of SNAP23. Next, we analyzed whether rescued AJC formation leads to RGC polarization, proliferation, and differentiation. Similar to those of the NcKO cortex, the radial processes were shortened or absent, and the basal bodies were diffusely localized throughout the VZ after electroporation of SNAP23 sgRNA and N-cadherin–mCherry (Fig. 6 A, arrowheads). In contrast, these features appeared normal after the electroporation of N-cadherin–LDLR–mCherry, suggesting that N-cadherin–LDLR rescued RGC polarity (Fig. 6 B, arrowheads). Moreover, the number of Pax6-positive RGCs and Tuj1-positive neurons in the VZ/sub-VZ was re-established by the electroporation of N-cadherin–LDLR–mCherry but not N-cadherin–mCherry (Fig. 6, C and D). Based on these results, we conclude that the decreased localization of N-cadherin to the apical PM is a primary cause of the severe dysplasia of the NcKO brain.

β-Catenin and Notch signaling are downregulated in the NcKO brain

Several components of AJCs are involved in regulating the signal transduction pathways of RGCs. For example, the signaling pathway mediated by β-catenin promotes RGC proliferation and inhibits neuronal differentiation (Chenn and Walsh, 2002; Zechner et al., 2003). In addition, Par3 regulates Notch signaling by interacting with Numb to inhibit neuronal differentiation (Bultje et al., 2009). Therefore, we speculated that the disruption of AJCs might lead to the inactivation of β-catenin and/or Notch signaling pathways. To confirm this, we investigated the levels of the active form of β-catenin and Notch1 intracellular domain (NICD), which is the cleaved active form of Notch1, in the NcKO brain at E13.5. The levels of active β-catenin and NICD were significantly decreased in the NcKO brain, although the levels of total β-catenin and full-length Notch1 were comparable in the control and NcKO brains (Fig. 7, A–D). In addition, mRNA expression of several target genes in each signaling pathway was decreased (Fig. 7, E and F). Therefore, the disruption of AJCs in the NcKO brain decreases the activities of the β-catenin and Notch signaling pathways, resulting in the abnormal differentiation of RGCs.

A previous report showed that the Notch pathway is also necessary for cell survival (Mason et al., 2006). Thus, the increased apoptosis in the NcKO brain is also likely caused by the down-regulation of Notch signaling. To address this, we attempted to rescue cells from apoptosis by increasing Notch activity through IUE of a plasmid encoding NICD. When we electroporated the mCherry plasmid, NICD plasmid, and reporter plasmid of Notch signaling, 12xCSL-d1EGFP, the number of GFP-positive cells was clearly increased in the VZ (Fig. 7 G). This result indicates that Notch signaling was upregulated by the expression of NICD. Next, we electroporated the NICD plasmid and Cas9 with the SNAP23 sgRNA plasmid to determine whether the downregulation of Notch signaling causes apoptosis in the NcKO brain. Similar to the results in the NcKO brain, TUNEL-positive cells were increased in the SNAP23-depleted region (Fig. 7, H and I). In contrast, the number of TUNEL-positive cells was decreased to less than half after coelectroporation of the NICD plasmid (Fig. 7, H and I). These results suggest that the increased cell death in the NcKO brain was mostly caused by the downregulation of Notch signaling.

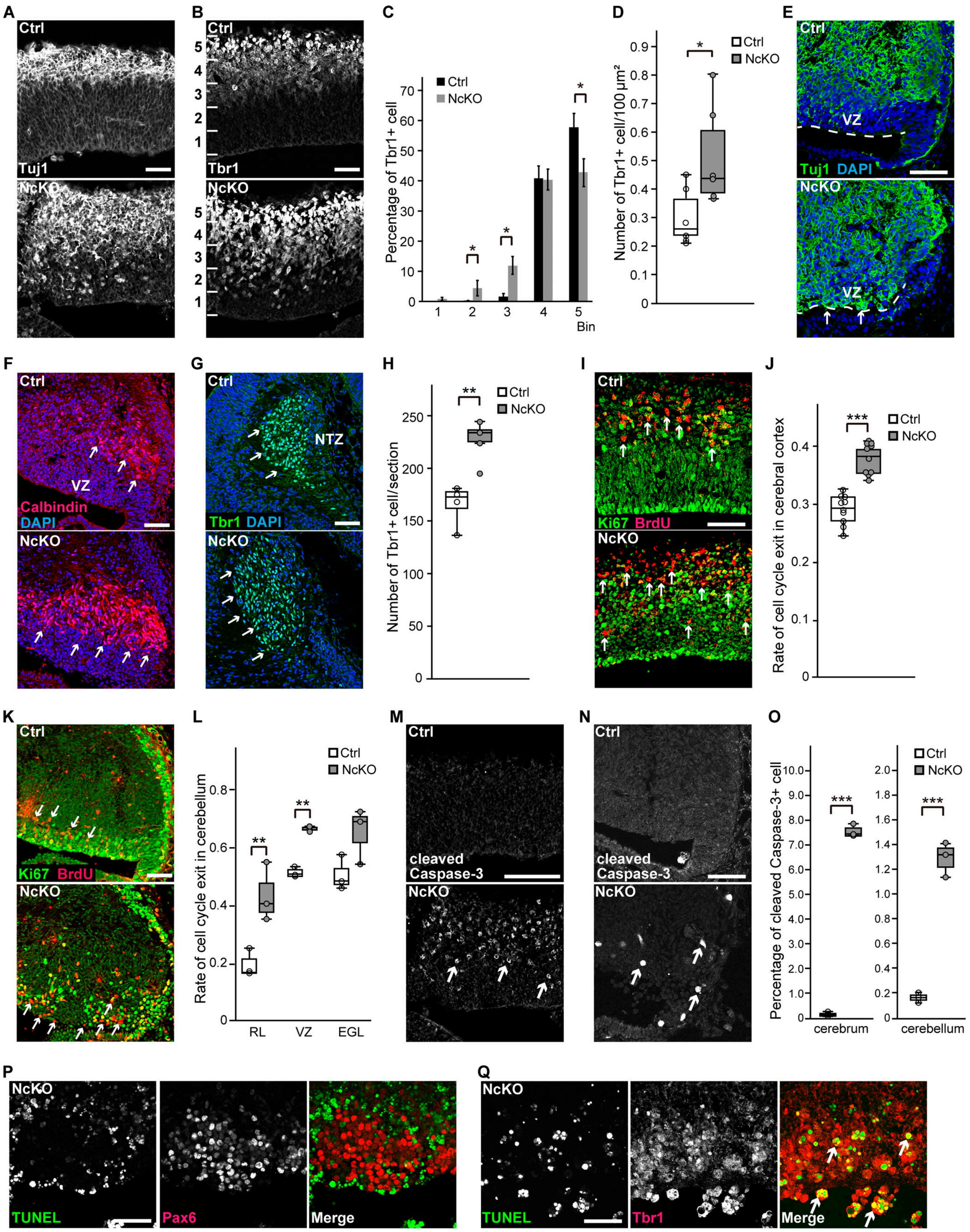
A
Ctrl
Tuj1
NcKO
B
Ctrl
5
4
3
2
1
Tbr1
NcKO
C
Percentage of Tbr1+ cell
Ctrl
NcKO
70
60
50
40
30
20
10
0
*
1
2
3
4
5
Bin
D
Number of Tbr1+ cell/100 µm²
0.9
0.8
0.7
0.6
0.5
0.4
0.3
0.2
0.1
0
E
VZ
Tuj1 DAPI
F
Calbindin
DAPI
G
NTZ
Tbr1 DAPI
H
Number of Tbr1+ cell/section
**
250
200
150
100
50
I
Ki67 BrdU
J
Rate of cell cycle exit in cerebral cortex
***
K
L
Rate of cell cycle exit in cerebellum
0.8
0.6
0.4
0.2
RL
VZ
EGL
M
cleaved
Caspase-3
N
O
Percentage of cleaved Caspase-3+ cell
10.0
9.0
8.0
7.0
6.0
5.0
4.0
3.0
2.0
1.0
0
cerebrum
2.0
1.8
1.6
1.4
1.2
1.0
0.8
0.6
0.4
0.2
cerebellum
P
TUNEL
Pax6
Merge
Q
TUNEL
Tbr1
Merge

Figure 3. **SNAP23 deficiency enhances neural differentiation and apoptosis. (A and B)** Tuj1 (A) or Tbr1 (B) stained in coronal sections of the cerebrum at E13.5. Scale bar, 50 µm. **(C)** Distribution of Tbr1-positive neurons in cerebral sections (*n* = 6 sections from three mice per genotype). **(D)** Density of Tbr1-

positive neurons in cerebral sections (*n* = 6 sections from three mice per genotype). **(E–G)** Tuj1 (green in E), Calbindin (red in F, arrows), or Tbr1 (green in G, arrows) and DAPI (blue) stained in sagittal sections of the cerebellum at E13.5. The dashed lines and arrows in E indicate the ventricular surface and the abnormal localization of Tuj1-positive cells, respectively. Scale bars, 50 µm. **(H)** Number of Tbr1-positive neurons in cerebellar sections (*n* = 4 sections from three mice per genotype). **(I)** Ki67 (green) and BrdU (red) stained in coronal sections of the cerebrum at E13.5. The arrows indicate cells that exited the cell cycle (BrdU positive and Ki67 negative). Scale bar, 50 µm. **(J)** Quantification of the cell cycle exit rate in cerebral sections (*n* = 10 sections from three mice per genotype). The number of BrdU-positive/Ki67-negative cells was divided by the total number of BrdU-positive cells. **(K)** Ki67 (green) and BrdU (red) stained in sagittal sections of the cerebellum at E13.5. The arrows indicate cells that exited the cell cycle. Scale bar, 50 µm. **(L)** Quantification of the cell cycle exit rate in cerebellar sections (*n* = 3 sections from three mice per genotype). **(M and N)** Cleaved Caspase-3 stained in coronal sections of the cerebrum (M) and in sagittal sections of the cerebellum (N) at E13.5. Arrows indicate cleaved Caspase-3–positive cells. Scale bars, 50 µm. **(O)** Percentage of cleaved Caspase-3–positive cells in cerebral and cerebellar sections (*n* = 3 sections from three mice per genotype). **(P and Q)** TUNEL and Pax6 (P) or Tbr1 (Q) stained in coronal sections of the cerebrum at E14.5. Tbr1 staining overlaps with TUNEL-positive dying cells (arrows). Scale bars, 50 µm. The box plots represent the maximum and minimum values. The centerlines of the box plots represent the medians of the data. The bar graphs represent the means ± SEM. Significance was calculated by using two-tailed paired Student's *t* tests. Statistical significance is indicated by *P < 0.05, **P < 0.01, or ***P < 0.001. Ctrl, control; EGL, external granular layer; NTZ, nuclear transitory zone; RL, rhombic lip; VZ, ventricular zone.

VAMP8 and Stx1B cooperate with SNAP23 to promote the localization of N-cadherin to the PM

SNAP23 is a Qbc-SNARE protein that forms a ternary complex with R- and Qa-SNARE proteins to promote membrane fusion between transport vesicles and the PM (Hong, 2005; Jahn and Scheller, 2006; Südhof and Rothman, 2009). We attempted to identify partner SNARE proteins of SNAP23 to determine the molecular mechanism underlying the localization of N-cadherin to the apical PM in RGCs. We performed an immunoprecipitation assay with E13.5 WT cerebral cortical lysates using a SNAP23 antibody and identified coprecipitated proteins using mass spectrometry. Seven SNARE proteins were detected as candidate binding proteins (Table S1). Among these candidates, we excluded Sec22b because it is localized at the ER (Hong, 2005). SNAP25 was also excluded because it does not bind SNAP23 (Kunii et al., 2016). SNAP25 might have been precipitated due to weak cross-reactivity with the SNAP23 antibody. The other five SNARE proteins were analyzed by knocking down each one with the respective siRNA (Fig. S2 A) to assess the adhesion between RGCs. The cell aggregation assays revealed a decreased number of VAMP8- and Stx1B-depleted RGC aggregates (Fig. S2, B and C). In the E13.5 WT cortex, VAMP8 and Stx1B are preferentially localized at the apical side of RGCs and are colocalized with N-cadherin (Fig. S1, A and C). Thus, we hypothesized that VAMP8 and Stx1B are the partner SNAREs for SNAP23 for the PM delivery of N-cadherin. Similar to the SNAP23-depleted RGCs, the VAMP8- or Stx1B-depleted RGCs were more dissociated, and the amount of N-cadherin at cell–cell contacts (Fig. 8, A–D) and at the cell surface (Fig. 8, E–G) was reduced. In contrast, depletion of VAMP3, -4, or -5 did not affect the PM localization of N-cadherin (Fig. S2 D).

Additional analyses were performed to confirm the functions of VAMP8 and Stx1B. First, we observed intracellular N-cadherin transport in living cells using a retention using selective hooks (RUSH) system (Boncompain et al., 2012). Since RGCs are too small and round to distinguish from vesicles in transport, we used COS7 cells. N-cadherin is abundantly expressed in COS7 cells, but E-cadherin is not highly expressed (Fig. 8 H). The amount of N-cadherin at cell–cell contacts was reduced, and the COS7 cells were dissociated by SNAP23, VAMP8, or Stx1B depletion, similar to the RGCs (Fig. 8, I–K). It suggests that these SNARE proteins are also involved in the localization of N-cadherin to the PM in COS7 cells.

COS7 cells were cotransfected with a plasmid encoding streptavidin-KDEL, an ER retention hook, and a plasmid encoding a streptavidin-binding peptide (SBP)–conjugated EGFP–N-cadherin reporter. SBP–EGFP–N-cadherin was retained in the ER in the absence of biotin. Fifteen minutes after the addition of biotin, SBP–EGFP–N-cadherin was observed in the Golgi apparatus, indicating that it was transported from the ER to the Golgi. It was further transported from the Golgi to the PM, as indicated by the PM localization of N-cadherin 60 min after biotin treatment (Fig. 9 A, arrows). The PM localization of SBP–EGFP–N-cadherin was confirmed by cell surface staining for EGFP (Fig. S3 A). The surface staining of EGFP was reduced in SNAP23-, VAMP8-, or Stx1B-depleted COS7 cells, suggesting that exogenously expressed N-cadherin was also delivered to the PM by these SNARE proteins (Fig. S3 A). We cotransfected a RUSH plasmid and a plasmid encoding mCherry–VAMP8 or mCherry–VAMP2 into COS7 cells to investigate whether the vesicles transporting N-cadherin from the Golgi to the PM also contained VAMP8. 60 min after biotin treatment, many of the SBP–EGFP–N-cadherin–positive vesicles were colocalized with mCherry–VAMP8 (Fig. 9, B and F). In contrast, the colocalization rate of the SBP–EGFP–N-cadherin–positive vesicles with mCherry–VAMP2 was significantly lower (Fig. 9, C and F). Previously, VAMP8 was shown to localize to lysosomes and to be involved in the fusion between autophagosomes and lysosomes (Itakura et al., 2012). However, the vesicles containing both SBP–EGFP–N-cadherin and mCherry–VAMP8 were not positive for LAMP2, a lysosome marker, suggesting that these vesicles were not lysosomes (Fig. S3 B, arrowheads). To confirm whether VAMP8 was preferentially localized to the N-cadherin–containing vesicles, we observed the colocalization of mCherry–VAMP8 or mCherry–VAMP2 with another type of transport vesicle. We used SBP–EGFP–glycosylphosphatidylinositol (GPI) because it is localized to the different vesicles from N-cadherin–containing vesicles (Fig. S3 C). 60 min after biotin treatment, many of the GPI-positive vesicles were colocalized with mCherry–VAMP2, but few of them were colocalized with mCherry–VAMP8 (Fig. 9, D–F). This result suggests that VAMP8 is preferentially localized to transport vesicles containing N-cadherin. Live cell imaging showed that EGFP–N-cadherin and mCherry–VAMP8 double-positive vesicles migrated to the cell surface (Fig. 9 G, arrows; and Video 2). Thus, N-cadherin was transported to the cell surface by VAMP8-positive transport vesicles.

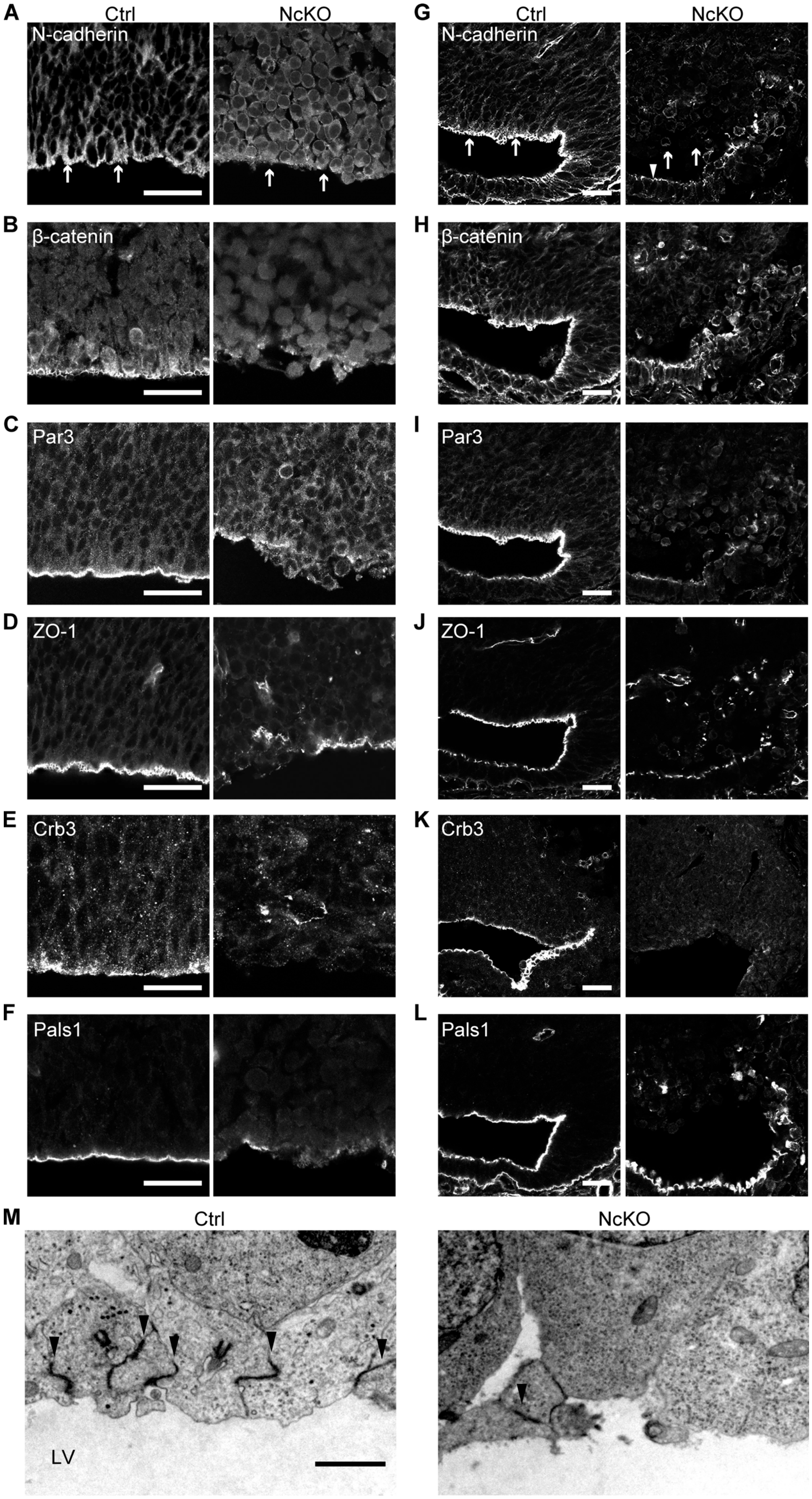
A
Ctrl
NcKO
N-cadherin
B
β-catenin
C
Par3
D
ZO-1
E
Crb3
F
Pals1
G
Ctrl
NcKO
N-cadherin
H
β-catenin
I
Par3
J
ZO-1
K
Crb3
L
Pals1
M
Ctrl
NcKO
LV

Figure 4. **SNAP23 deficiency disrupts AJCs in RGCs. (A–L)** N-cadherin (A and G), β-catenin (B and H), Par3 (C and I), ZO-1 (D and J), Crb3 (E and K), and Pals1 (F and L) stained in coronal sections of the cerebrum (A–F) or in sagittal sections of the cerebellum (G–L) at E13.5. Scale bars, 20 µm. Arrows in A and G indicate the ventricular surface. The arrowhead in G indicates the surface of the choroid plexus. Staining revealed that each marker remained at the surface of the choroid plexus in the NcKO mice because SNAP23 was not depleted in this region (see also Fig. 1 M). **(M)** Electron micrographs of the lateral ventricular (LV) surface of the cerebral cortex at E13.5. The electron-dense lines indicate that AJCs (arrowheads) were rarely observed in the NcKO cortex. Scale bar, 5 µm. Ctrl, control.

Next, to determine whether VAMP8 and Stx1B participate in AJC formation in vivo, we knocked out VAMP8 or Stx1B in the E13.5 cerebral cortex through the IUE of Cas9 and sgRNA plasmids. After VAMP8 or Stx1B sgRNA electroporation, apical ZO-1 staining became less intense, suggesting that the AJCs were disrupted (Fig. 10, A and B; and Fig. S4, B and C). Similar to the NcKO cortex, the boundary of the ventricular surface became irregular in the depleted region of the cerebral cortex (Fig. 10, A and B, arrows). These phenotypes were not observed when we electroporated SNAP25 sgRNA (Fig. S5, A and B). Because the expression of SNAP25 is low in RGCs (Fig. S1 B), SNAP25 may not have a function in N-cadherin transport in RGCs.

In our immunoprecipitation assay, Stx1B was the only Qa-SNARE protein that coprecipitated with SNAP23. Previous reports showed that Stx1B KO mice did not present morphological defects in their brain structure (Mishima et al., 2014; Wu et al., 2015). A homologous protein, Stx1A, may compensate for the loss of Stx1B. Indeed, a recent study showed a wide range of malformations in brain structures in mice lacking both Stx1A and Stx1B, suggesting that Stx1A and/or Stx1B are involved in brain development (Vardar et al., 2016). Therefore, we examined the function of Stx1A in N-cadherin transport. Although Stx1A was not detected by mass spectrometry among the proteins that coprecipitated with SNAP23, it was detected by immunoblotting (Fig. S5 C). However, knocking out Stx1A through IUE showed normal Par3 staining and a smooth ventricular surface, suggesting that AJC formation was unaffected (Fig. S5 D). These data suggest that Stx1B is a major Qa-SNARE that acts on N-cadherin transport in RGCs. Altogether, we conclude that VAMP8 and Stx1B are involved in the delivery of N-cadherin to the PM and in the subsequent AJC formation in RGCs.

Discussion

In this study, we show that SNAP23 and its partner SNAREs, VAMP8 and Stx1B, are essential for the development of the mouse brain.

SNAP23 depletion resulted in decreased localization of several proteins, including N-cadherin, to the PM (Fig. 5), suggesting that SNAP23 is necessary for the PM localization of these proteins in RGCs. The perturbed localization of many PM proteins might be involved in the dysplasia of the NcKO brain; however, the results of rescue experiments using N-cadherin–LDLR (Figs. 5 and 6) indicated that the decreased localization of N-cadherin at the PM was likely a primary cause of the severe dysplasia. Decreased localization of N-cadherin at the apical PM would lead to AJC formation failure, which would be followed by perturbed apico-basal polarization. The loss of AJCs and RGC polarity leads to the abnormal proliferation and differentiation of RGCs and to the apoptosis of neurons through the downregulation of β-catenin and Notch signaling.

In addition to that of N-cadherin, the PM localization of β1-integrin and Ephrin-B1 was reduced in the SNAP23-depleted RGCs (Fig. 5, C and D). These proteins are important for the contacts established between the RGC basal process and the basement membrane and for the progenitor state of the RGCs, respectively (Graus-Porta et al., 2001; Qiu et al., 2008). Thus, decreased localization of these proteins may exacerbate the dysplasia of the NcKO brain, as indicated by the extent of dysplasia appearing to be more severe in the NcKO mice than in the N-cadherin–depleted mice (Kadowaki et al., 2007).

In contrast to β1-integrin or Ephrin-B1, the PM localization of LDLR and Na^+/K^+-ATPase was relatively unaffected (Fig. 5, C and D). These molecules may be delivered by the other SNAP25 family proteins, such as SNAP29 or SNAP47 (Kádková et al., 2019). The mechanism of cargo selectivity of SNARE proteins remains unknown; however, the results of our rescue experiments by N-cadherin–LDLR suggest that differences in the sequence of the TMD or sorting motifs in the cytoplasmic region, such as the di-leucine motif in N-cadherin (Miranda et al., 2001) or tyrosine-containing motifs and NPxY motif in LDLR (Burden et al., 2004; Matter et al., 1992), may be required for selectivity.

We found that VAMP8 and Stx1B are also important for N-cadherin transport in RGCs. VAMP8 is involved in zymogen granule exocytosis in exocrine cells (Wang et al., 2004, 2007); however, its function in the CNS remains unknown. We found that VAMP8 was preferentially localized to N-cadherin–transporting vesicles and moved to the cell surface (Fig. 9 and Video 2). Moreover, CRISPR/Cas9 KO of VAMP8 caused AJC disruption in the cerebral cortex (Fig. 10 A). These results indicate that VAMP8 is necessary for the trafficking of N-cadherin and AJC formation in RGCs.

Previously, the loss of Dlg5, a component of the Scribble polarity complex (Assémat et al., 2008), was reported to induce hydrocephalus through the disruption of AJCs and the loss of RGC polarity in the developing cortex (Nechiporuk et al., 2007). A Qa-SNARE protein, Stx4, interacts with Dlg5 in the brain and mouse embryonic fibroblasts. The amount of N-cadherin at the cell surface was decreased in Dlg5-null mouse embryonic fibroblasts, suggesting that Dlg5 and Stx4 promote the localization of N-cadherin to the PM (Nechiporuk et al., 2007). In our study, another Qa-SNARE protein, Stx1B, coprecipitated with SNAP23. Furthermore, the amount of N-cadherin at the PM was markedly decreased in the Stx1B-depleted RGCs (Fig. 8). Thus, Stx1B is also important for promoting the localization of N-cadherin to the apical PM by forming a SNARE complex with SNAP23 and VAMP8.

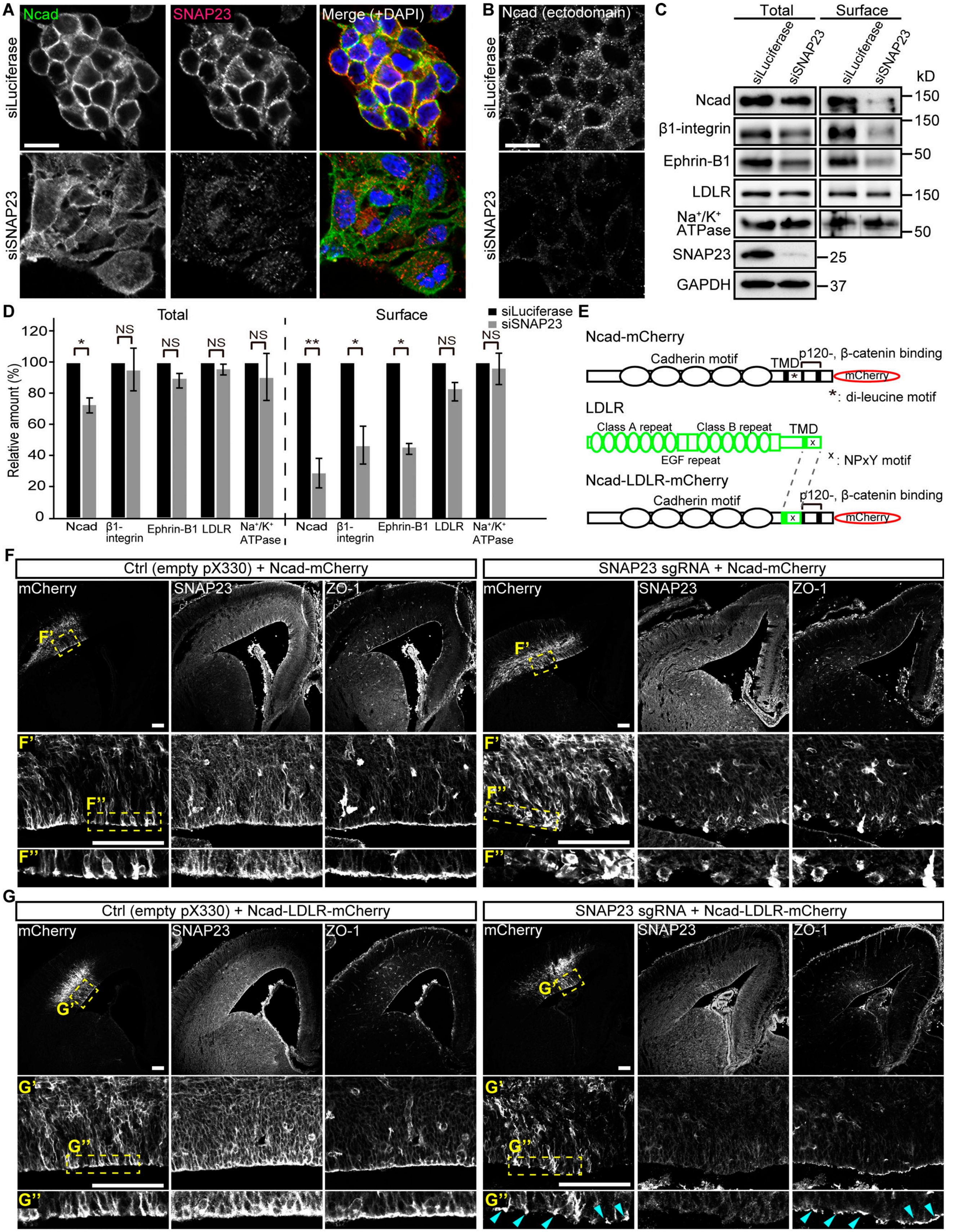
A
Ncad
SNAP23
Merge (+DAPI)
siLuciferase
siSNAP23
B
Ncad (ectodomain)
siLuciferase
siSNAP23
C
Total
Surface
siLuciferase
siSNAP23
siLuciferase
siSNAP23
kD
Ncad
β1-integrin
Ephrin-B1
LDLR
Na⁺/K⁺ ATPase
SNAP23
GAPDH
150
150
50
150
50
25
37
D
Total
Surface
siLuciferase
siSNAP23
Relative amount (%)
120
100
80
60
40
20
0
*
NS
NS
NS
NS
**
*
*
NS
NS
Ncad
β1-integrin
Ephrin-B1
LDLR
Na⁺/K⁺ ATPase
Ncad
β1-integrin
Ephrin-B1
LDLR
Na⁺/K⁺ ATPase
E
Ncad-mCherry
Cadherin motif
TMD
p120-, β-catenin binding
mCherry
*: di-leucine motif
LDLR
Class A repeat
Class B repeat
TMD
EGF repeat
x: NPxY motif
Ncad-LDLR-mCherry
Cadherin motif
p120-, β-catenin binding
mCherry
F
Ctrl (empty pX330) + Ncad-mCherry
SNAP23 sgRNA + Ncad-mCherry
mCherry
SNAP23
ZO-1
F'
F''
G
Ctrl (empty pX330) + Ncad-LDLR-mCherry
SNAP23 sgRNA + Ncad-LDLR-mCherry
mCherry
SNAP23
ZO-1
G'
G''

Figure 5. **Knockdown of SNAP23 decreases the PM localization of N-cadherin in cultured RGCs. (A)** N-cadherin (Ncad; green) and SNAP23 (red) stained with DAPI (blue) in the control (Ctrl; siLuciferase) and SNAP23-depleted RGCs. Scale bar, 10 µm. **(B)** N-cadherin ectodomain stained in the Ctrl and SNAP23-depleted

RGCs. Scale bar, 10 µm. **(C and D)** Immunoblots showing the levels of total and cell surface N-cadherin, β1-integrin, Ephrin-B1, LDLR, and Na$^+$/K$^+$-ATPase in the Ctrl and SNAP23-depleted RGCs. Relative expression was calculated from three independent experiments. **(E)** Diagrams of N-cadherin–mCherry and N-cadherin–LDLR–mCherry. **(F and G)** SNAP23 and ZO-1 stained in the SNAP23 sgRNA and N-cadherin–mCherry (F) or N-cadherin–LDLR–mCherry (G) electroporated region of the cerebral cortex. An empty pX330 plasmid was electroporated as a control. mCherry staining shows the electroporated region. Lower panels (F′, F′′, G′, and G′′) show magnified images of the boxes surrounded by dashed lines in the upper panels. Arrowheads in G′′ indicate staining of recovered ZO-1. Scale bars, 100 µm. The bar graphs represent the means ± SEM. Significance was calculated using two-tailed paired Student's *t* tests. Statistical significance is indicated by $^*P < 0.05$ or $^{**}P < 0.01$.

In summary, we revealed a function for a SNARE complex composed of SNAP23, VAMP8, and Stx1B in promoting the localization of N-cadherin to the apical PM in RGCs. This complex is necessary for the polarization of RGCs and subsequent normal brain development (Fig. 10 C). However, the detailed mechanisms of the SNARE-mediated organization of AJCs are not yet understood; therefore, additional investigations should be performed to elucidate the functions of other SNAREs during brain development.

Materials and methods

Mice

Snap23$^{f/f}$ mice (Kunii et al., 2016) were crossed with Nestin-Cre mice (Tronche et al., 1999; The Jackson Laboratory) to obtain CNS-specific *Snap23* KO mice (Nestin-Cre; *Snap23*$^{floxed/-}$ or $^{floxed/floxed}$ abbreviated as NcKO). *Snap23*$^{floxed/-}$ or $^{floxed/floxed}$ mice were used as controls. All animal experiments were performed in accordance with the guidelines of the Animal Care and Experimentation Committees of Gunma University and Osaka University. The genotypes of the mice were identified by PCR using the following primers: primer 1 (5′-CTGGGGAATGTGCGTTTGGATGATG-3′); primer 2 (5′-CCCCTTTCATCATGCTTCAAATGCAACC-3′); primer 3 (5′-TGTTCCTGGATTGAGCTCAGGTGGT-3′); primer 4 (5′-AGGTTCGTTCTCTCATGGA-3′); and primer 5 (5′-TCGACCAGTTTAGTTACCC-3′). Primers 1 and 2, primers 2 and 3, and primers 4 and 5 were used for the floxed allele, the null allele, and the *cre* gene, respectively.

Histology

Most of the procedures used for histological experiments were described previously (Kunii et al., 2016). For hematoxylin-eosin staining, E16.5 and P0 mice were intracardially perfused with 3% paraformaldehyde in 0.1 M phosphate buffer (pH 7.4). The heads were subjected to additional fixation in the same fixative for 2 h. After fixation, each head was dehydrated in ethanol and embedded in paraffin. The skull bone was not removed to protect the abnormal structure of the NcKO brain. Paraffin-embedded tissue sections (4 µm) were stained with a solution of hematoxylin-eosin. For Nissl staining of the brain sections, embryos were fixed with 3% paraformaldehyde in 0.1 M phosphate buffer. Heads were embedded in O.C.T. Compound (Sakura Finetek) and frozen in liquid nitrogen–chilled isopentane. Frozen sections were cut using a cryostat (Leica) and stained with a toluidine blue solution. For immunofluorescence staining, frozen sections were labeled with primary and secondary antibodies as described below. TUNEL staining was performed using a DeadEnd Fluorometric TUNEL system (Promega) according to the manufacturer's instructions. Confocal images were obtained using an Olympus FV1000D laser-scanning microscope (Olympus) with UPLSAPO 10×, 20×, 60×, and 100× objective lenses (NA 0.40, 0.75, 1.35, and 1.40, respectively; Olympus). For EM, E13.5 control and NcKO embryos were intracardially perfused with 2.5% glutaraldehyde and 2% paraformaldehyde in 0.1 M cacodylate buffer (pH 7.4). The brains were fixed in the same fixative and then placed in 1% OsO_4. The tissues were then incubated with 0.5% uranyl acetate in H_2O, dehydrated, and embedded in Quetol-812 (Nisshin EM). Ultrathin sections were cut using an ultramicrotome (Reichert-Jung). Electron micrographs were captured using a JEM1010 instrument (JEOL).

Antibodies

The following primary and secondary antibodies were used: anti-SNAP23 (rabbit; Kunii et al., 2016), anti-SNAP25 (mouse; Covance, SMI-81R), anti-Nestin (mouse; BD Pharmingen, 556309), anti-Pax6 (rabbit; COVANCE, PRB-278P), anti-Pericentrin (rabbit; Covance, PRB-432C), anti-PH3 (rabbit; Upstate, 06-570), anti-Tuj1 (mouse; Covance, MMS-435P), anti-Tbr1 (rabbit; Millipore, AB10554), anti-Calbindin (goat; Santa Cruz Biotechnology, sc-7691), anti-Ki67 (rabbit; Novo Castra, NCL-Ki67p), anti-BrdU (mouse; BD Pharmingen, 555627), anti–cleaved caspase-3 (rabbit; Cell Signaling Technology, 9661), anti–N-cadherin (mouse; BD Transduction, 610920), anti–N-cadherin ectodomain (mouse; Sigma-Aldrich, C3865), anti–E-cadherin (mouse; BD Transduction, 610181), anti–total β-catenin (mouse; BD Transduction, 610153), anti–active β-catenin (mouse; Upstate, 05-665), anti-Par3 (rabbit; Upstate, 07-330), anti–ZO-1 (mouse; Zymed, 33-9100), anti-Crb3 (rabbit; a kind gift from Dr. Dominique Massey-Harroche, Aix-Marseille University, Marseille, France), anti-Pals1 (mouse; Santa Cruz Biotechnology, sc-365411), anti–β1-integrin (rat; Chemicon, MAB1997), anti–ephrin-B1 (goat; R&D Systems, AF473), anti-LDLR (goat; R&D Systems, AF2255), anti–Na$^+$/K$^+$-ATPase β subunit (rabbit antisera; a kind gift from Dr. Haruo Homareda, Kyorin University, Mitaka, Tokyo, Japan), anti-mCherry (rat; Invitrogen, M11217), anti-Notch1 (rabbit; Cell Signaling Technology, 3608), anti–cleaved Notch1 (rabbit; Cell Signaling Technology, 2421), anti-VAMP3 (rabbit; Synaptic Systems, 104102), anti-VAMP4 (rabbit; Invitrogen, PA1-768), anti-VAMP5 (rabbit; Synaptic Systems, 176003), anti-VAMP8 (rabbit; Synaptic Systems, 104302), anti-Syntaxin1A (mouse; Sigma-Aldrich, S0664), anti-Syntaxin1B (rabbit; Synaptic Systems, 110402), anti-Lamp2 (mouse; Developmental Studies Hybridoma Bank, H4B4), anti-GAPDH (mouse; Calbiochem, CB1001), anti–Lamin B (mouse; Santa Cruz Biotechnology, sc-374015), Alexa 488–, 568–, and Cy5-labeled donkey anti-rabbit, anti-mouse, and anti-rat IgG (Molecular Probes), and HRP-labeled donkey anti-rabbit,

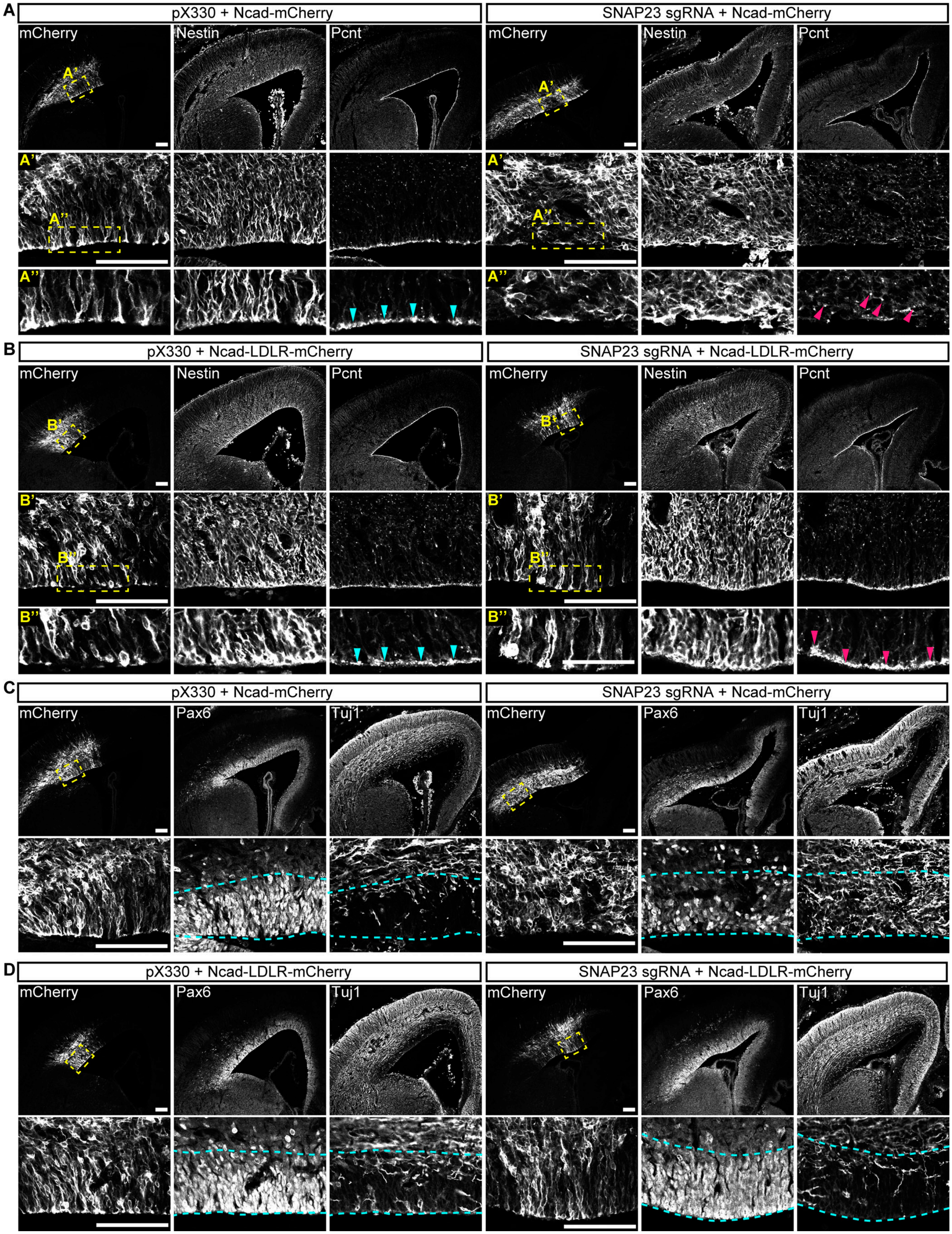
A
pX330 + Ncad-mCherry
SNAP23 sgRNA + Ncad-mCherry
mCherry
Nestin
Pcnt
A'
A''
B
pX330 + Ncad-LDLR-mCherry
SNAP23 sgRNA + Ncad-LDLR-mCherry
B'
B''
C
pX330 + Ncad-mCherry
SNAP23 sgRNA + Ncad-mCherry
Pax6
Tuj1
D
pX330 + Ncad-LDLR-mCherry
SNAP23 sgRNA + Ncad-LDLR-mCherry

Figure 6. **N-cadherin-LDLR rescues abnormal polarity, proliferation, and differentiation of RGCs in the SNAP23-depleted cortex. (A and B)** Nestin and Pericentrin (Pcnt) stained in the SNAP23 sgRNA and N-cadherin (Ncad)–mCherry (A) or Ncad–LDLR–mCherry (B) electroporated region of the cerebral cortex. pX330 was electroporated as a control. mCherry staining shows the electroporated region. Lower panels (A′, A′′, B′, and B′′) show magnified images of the boxes surrounded by dashed lines in the upper panels. Arrowheads in A′′ and B′′ indicate the localization of basal bodies. Scale bars, 100 µm. **(C and D)** Pax6 and Tuj1 stained in the SNAP23 sgRNA and Ncad–mCherry (C) or Ncad–LDLR–mCherry (D) electroporated region of the cerebral cortex. pX330 was electroporated as a control. mCherry staining shows the electroporated region. Lower panels show magnified images of the boxes surrounded by dashed lines in the upper panels. The area between two blue dashed lines indicates the VZ/sub-VZ. Scale bars, 100 µm.

---

anti-mouse, anti-rat, and anti-goat IgG (Jackson ImmunoResearch Laboratories).

Immunoblotting

E12.5 and E13.5 embryonic brains, primary RGCs, or COS7 cells were homogenized in lysis buffer (80 mM Tris-HCl, pH 6.8, and 2% SDS) containing a protease inhibitor cocktail (Wako Chemicals). The lysates were subsequently boiled and centrifuged at 20,000× *g* for 10 min. The supernatants were then used for immunoblotting using the specific antibodies noted above. The procedures for SDS-PAGE and immunoblotting were described previously (Kunii et al., 2016). Chemiluminescent images were obtained using LAS4000 (GE Healthcare). For the immunoblotting of VAMP5 and VAMP8, NOVEX 10–20% Tricine gels (Invitrogen) and Immobilon PSQ membranes (Millipore) were used.

Quantitative real-time PCR

Total RNA was extracted from the embryonic brain using NucleoSpin RNA kit (Macherey-Nagel) according to the manufacturer's instructions. First-strand cDNA was synthesized by random primers (6mers) and reverse transcription (Takara). Quantitative real-time PCR was performed using a ViiA7 instrument (Applied Biosystems). Universal Probes #50, #22, and #78 (Roche) were used for *Axin2*, *Hes5*, and glucose-6-phosphate dehydrogenase X-linked (*G6pdx*), respectively. The following primers were used for PCR: *Axin2* sense (5′-CCATGACGGACA GTAGCGTA-3′); *Axin2* antisense (5′-GCCATTGGCCTTCACACT-3′); *Hes5* sense (5′-CCCAAGGAGAAAAACCGACT-3′); *Hes5* antisense (5′-TGCTCTATGCTGCTGTTGATG-3′); *G6pdx* sense (5′-GA AAGCAGAGTGAGCCCTTC-3′); and *G6pdx* antisense (5′-CATAG GAATTACGGGCAAGA-3′).

Immunoprecipitation and mass spectrometry analysis

Immunoprecipitation was performed as previously described (Kunii et al., 2016). Briefly, the neocortical tissues from E13.5 WT mice were dissociated with 0.25% trypsin in PBS and incubated with 1 mM *N*-ethylmaleimide in PBS for 30 min at 37°C. Cells were lysed in NP-40 lysis buffer (1% NP-40, 25 mM Hepes, pH 7.4, 10% glycerol, 137 mM NaCl, and a protease inhibitor cocktail). 2 mg cleared lysate was mixed with protein G Sepharose beads (GE Healthcare), which bind the anti-SNAP23 antibody or the control rabbit IgG, and was rotated for 2 h at 4°C. The Sepharose beads were washed three times with lysis buffer. The precipitated products were eluted with 0.2 M glycine-HCl, pH 2.0, and neutralized with Tris-HCl, pH 9.5. The eluted samples were analyzed by immunoblotting or mass spectrometry using a Q-Exactive mass spectrometer (Thermo Fisher Scientific) at Osaka University Center for Medical Innovation and Translational Research. A database search was performed using Mascot Distiller v2.4 and Mascot Server v2.4 (Matrix Science).

Culture of primary RGCs

Neocortical RGCs were collected from E13.5 embryos using previously described methods (Sakakibara et al., 1996). Briefly, the neocortex was isolated from E13.5 WT mouse using tungsten needles and dissociated with trypsin (0.25% in PBS for 10 min at 37°C). The isolated RGCs were cultured in DMEM/Ham's F-12 containing N2 supplement (Gibco), 5% horse serum, 5% FCS, FGF (1 µg/ml; PeproTech), and EGF (1 µg/ml; PeproTech), with astrocytes from the E18.5 neocortex serving as feeder cells. For the knockdown of each SNARE protein, the following siRNAs (Sigma-Aldrich) were transfected into cells with Lipofectamine RNAiMAX (Invitrogen): Luciferase siRNA: 5′-AAACAUGCAGAA AAUGCUGtt-3′; SNAP23 siRNA#1: 5′-GGCAUGGACCAAAUAA AUAtt-3′; SNAP23 siRNA#2: 5′-CAUUAAACGUAUAACUAAUGAt t-3′; VAMP3 siRNA#1: 5′-GCUCAUGCUCUUAUGUUAGtt-3′; VAMP3 siRNA#2: predesigned MISSION siRNA oligo (SASI_Mm02_00316256); VAMP4 siRNA#1: 5′-CGUACGUUUGAG CUUAUAAtt-3′; VAMP4 siRNA#2: predesigned MISSION siRNA oligo (SASI_Mm01_00172967); VAMP5 siRNA#1: 5′-GGGAAG GCUGAAUGACUGC-3′; VAMP5 siRNA#2: predesigned MISSION siRNA oligo (SASI_Mm02_00293595); VAMP8 siRNA#1: 5′-GCC ACGUCUGAACACUUCAtt-3′; VAMP8 siRNA#2: predesigned MISSION siRNA oligo (SASI_Mm01_00101527); Stx1B siRNA#1: mixture of three different predesigned MISSION siRNA oligos (SASI_Mm02_00327730, SASI_Mm01_00025452, and SASI_Mm01_00025454); and Stx1B siRNA#2: predesigned MISSION siRNA oligo (SASI_Mm02_00327729).

Cell aggregation assay

The ability of RGCs to aggregate was assessed using a previously described method (Thoreson et al., 2000). Briefly, control RGCs and all SNARE-depleted RGCs were trypsinized and resuspended at a density of 5 × 10^5 cells/ml in the culture medium described above. 30 µl of medium was suspended as hanging drops from the lid of a 24-well plate, with or without 5 mM EGTA, and incubated at 37°C for 18 h. After incubation, the density of the aggregates was calculated.

Cell surface biotinylation assay

Biotinylation of RGC surface proteins was performed as previously described (Atik et al., 2014). Briefly, the control and SNAP23-, VAMP8-, or Stx1B-depleted RGCs were washed with ice-cold PBS and incubated with PBS containing 0.5 mg/ml sulfo-NHS-LC-biotin (Thermo Fisher Scientific) at 4°C for

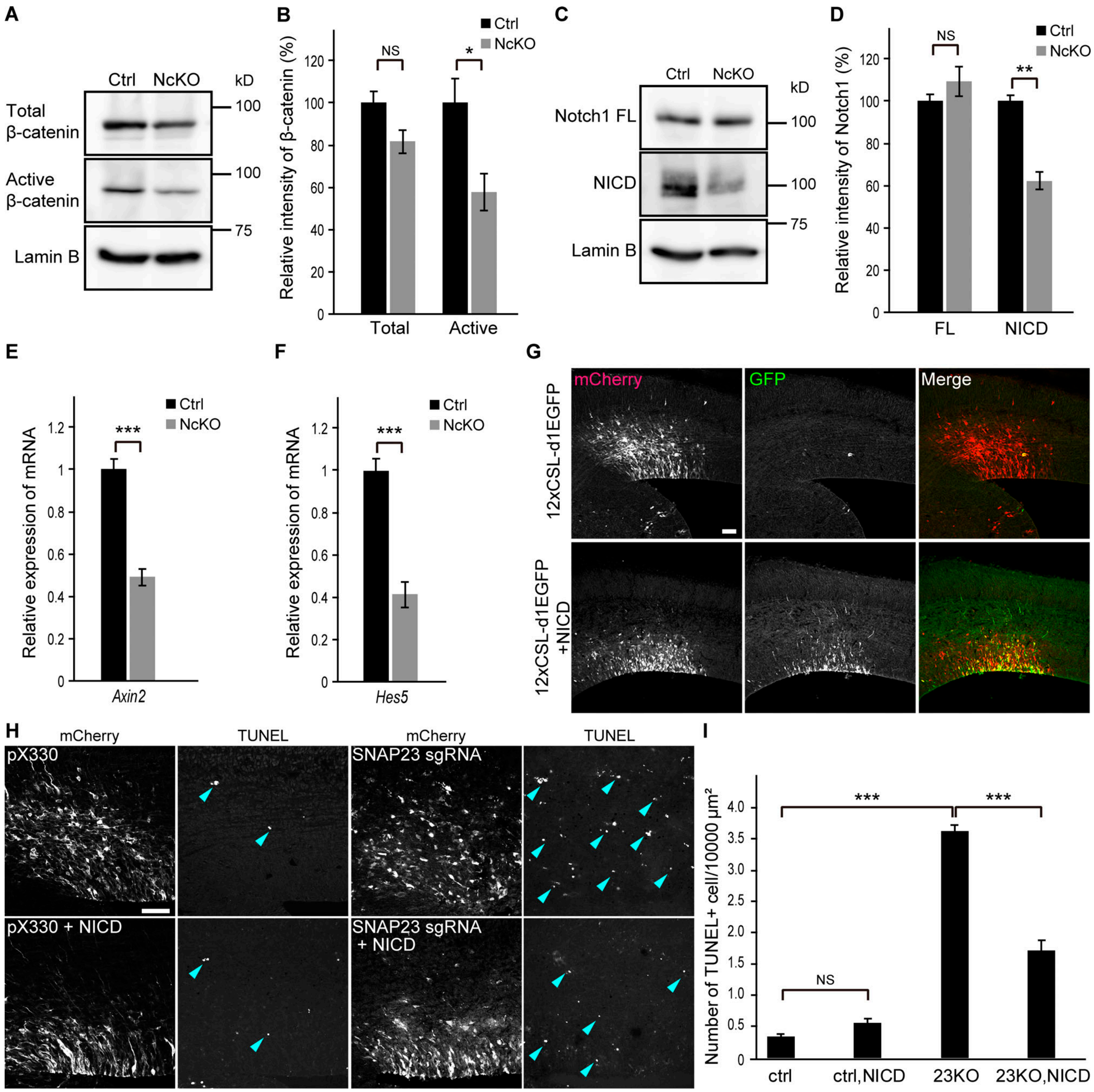

Figure 7. **SNAP23 deficiency decreases β-catenin and Notch signaling. (A and B)** Immunoblots showing the levels of total and active β-catenin in the control (Ctrl) and NcKO brains at E13.5. Lamin B blotting was used as a loading control. **(C and D)** Immunoblots showing the full-length (FL) and cleaved Notch1 (NICD) levels in the Ctrl and NcKO brains at E13.5. Lamin B blotting was used as a loading control. **(E and F)** Relative expression of *Axin2* and *Hes5* mRNA in the Ctrl and NcKO brains at E13.5, as measured with real-time PCR (*n* = 5 mice per genotype). **(G)** d1EGFP expression in the cerebral cortex with or without NICD plasmid. Scale bar, 200 µm. **(H)** TUNEL stained in the electroporated region of the cerebral cortex. pX330 was electroporated as a control. The mCherry plasmid was electroporated to show the electroporated region. The blue arrowheads indicate TUNEL-positive cells. Scale bar, 50 µm. **(I)** Density of TUNEL-positive cells in the electroporated region of the cerebral cortex (*n* = 5 sections from three mice per genotype).

30 min. The cells were washed twice with cold PBS and quenched with 50 mM NH_4Cl in PBS for 15 min at 4°C. Cells were washed again and lysed with 0.5% Triton X-100 in PBS. The cleared lysate was incubated with 10 µl of streptavidin beads (SoluLINK) for 1 h at 4°C. The beads were washed three times with 0.1% Triton X-100 in PBS, and the bound proteins were analyzed by immunoblotting with the specific antibodies noted above.

Time-lapse imaging of N-cadherin transport

COS7 cells were cultured in DMEM containing 10% FCS. For the knockdown of each SNARE protein, the following siRNAs (Sigma-Aldrich) were transfected into the cells with Lipofectamine RNAiMAX (Invitrogen): Luciferase siRNA: 5′-AAACAUGCAGAAAAUGCUGtt-3′; SNAP23 siRNA: predesigned MISSION siRNA oligo (SASI_Hs02_00362830); VAMP8 siRNA: predesigned MISSION siRNA oligo (SASI_Hs01_00159297);

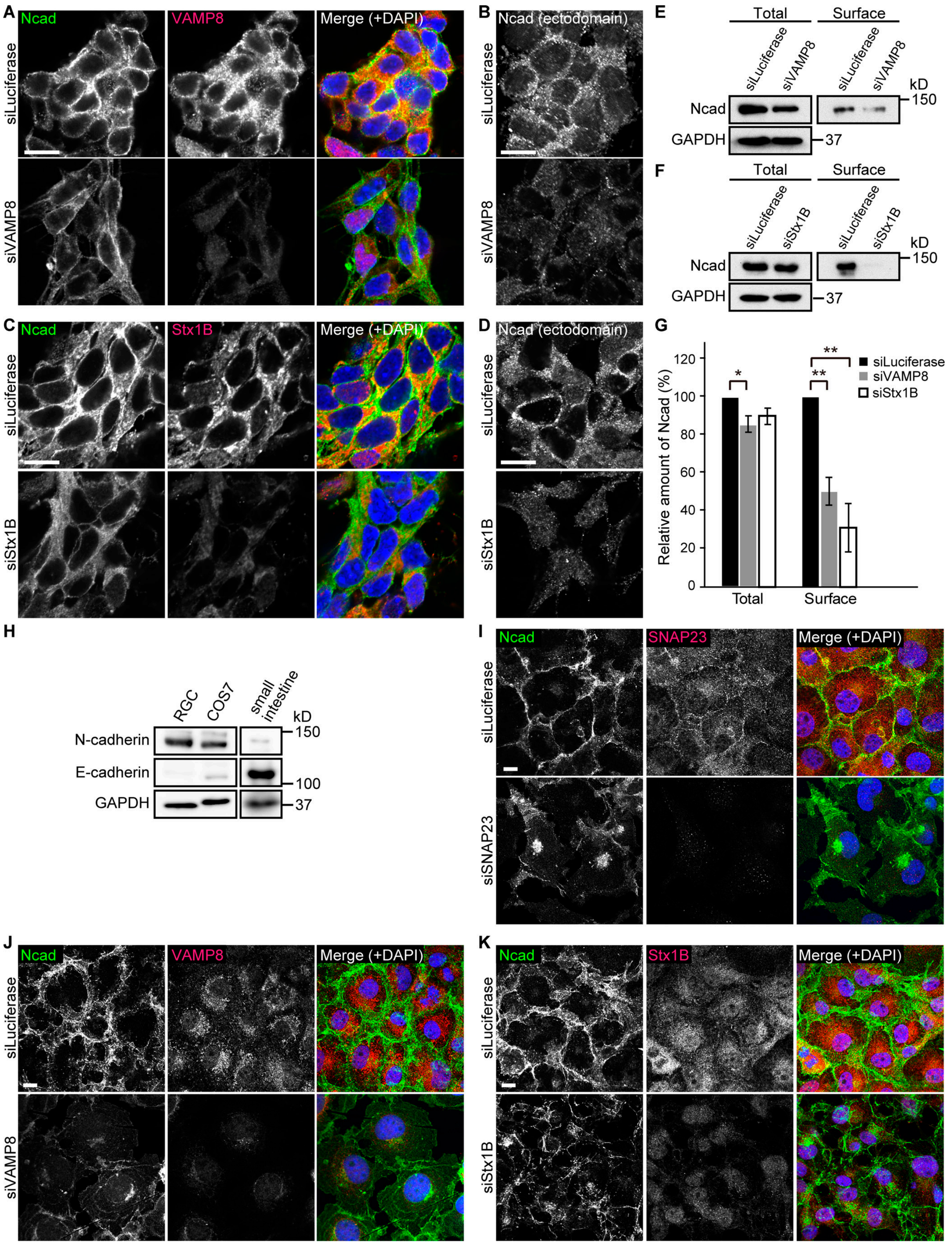
A
Ncad
VAMP8
Merge (+DAPI)
siLuciferase
siVAMP8
B
Ncad (ectodomain)
siLuciferase
siVAMP8
E
Total
Surface
siLuciferase
siVAMP8
siLuciferase
siVAMP8
kD
Ncad
150
GAPDH
37
F
Total
Surface
siLuciferase
siStx1B
siLuciferase
siStx1B
kD
Ncad
150
GAPDH
37
C
Ncad
Stx1B
Merge (+DAPI)
siLuciferase
siStx1B
D
Ncad (ectodomain)
siLuciferase
siStx1B
G
Relative amount of Ncad (%)
0
20
40
60
80
100
120
*
**
**
siLuciferase
siVAMP8
siStx1B
Total
Surface
H
RGC
COS7
small intestine
kD
N-cadherin
150
E-cadherin
100
GAPDH
37
I
Ncad
SNAP23
Merge (+DAPI)
siLuciferase
siSNAP23
J
Ncad
VAMP8
Merge (+DAPI)
siLuciferase
siVAMP8
K
Ncad
Stx1B
Merge (+DAPI)
siLuciferase
siStx1B

Figure 8. **Knockdown of VAMP8 or Stx1B decreases the localization of N-cadherin at the PM in cultured RGCs and COS7 cells. (A)** N-cadherin (Ncad; green) and VAMP8 (red) stained with DAPI (blue) in the control (siLuciferase) and VAMP8-depleted RGCs. Scale bar, 10 µm. **(B)** N-cadherin ectodomain stained in the control and VAMP8-depleted RGCs. Scale bar, 10 µm. **(C)** N-cadherin (green) and Stx1B (red) stained with DAPI (blue) in the control and Stx1B-depleted RGCs. Scale bar, 10 µm. **(D)** N-cadherin ectodomain stained in the control and Stx1B-depleted RGCs. Scale bar, 10 µm. **(E–G)** Immunoblots showing the levels of total and cell surface N-cadherin in control and VAMP8- (E) or Stx1B-depleted (F) RGCs. Relative levels of N-cadherin were calculated from three independent experiments. **(H)** Immunoblots showing N-cadherin and E-cadherin in the WT RGCs, COS7 cells, and mouse small intestines. GAPDH blotting was used as a loading control. **(I–K)** Ncad and SNAP23 (I), VAMP8 (J), or Stx1B (K) stained in the control and SNAP23-, VAMP8-, or Stx1B-depleted COS7 cells. Scale bars, 10 µm. The bar graphs represent the means ± SEM. Significance was calculated using two-tailed paired Student's *t* tests. Statistical significance is indicated by $^{*}P < 0.05$ or $^{**}P < 0.01$.

---

and Stx1B siRNA: predesigned MISSION siRNA oligo (SASI_Hs01_00179361).

RUSH plasmids (streptavidin-KDEL_SBP-EGFP-E-cadherin and streptavidin-KDEL_SBP-EGFP/mCherry-GPI; Boncompain et al., 2012) were kind gifts from Dr. Franck Perez (Curie Institute, Paris, France). We replaced the E-cadherin coding sequence with the N-cadherin sequence. COS7 cells were seeded on 35-mm glass-bottom dishes. A RUSH plasmid (streptavidin-KDEL_SBP-EGFP-N-cadherin or streptavidin-KDEL_SBP-EGFP/mCherry-GPI) and the mCherry–VAMP8 or mCherry–VAMP2 plasmid were cotransfected into COS7 cells, which were subsequently incubated for 20 h at 37°C. The cells were treated with 40 µM D-biotin (Sigma-Aldrich) and 0.1 mM cycloheximide. Live-cell imaging was performed using an SD-OSR microscope (Olympus) with a UPLSAPO 100XS objective lens (NA 1.35; Olympus). Time-lapse images were obtained every 10 s for 60 min at 37°C. 60 min after the biotin treatment, the cells were fixed with 3% PFA. Colocalization of the RUSH reporter (SBP–EGFP–N-cadherin or SBP–EGFP–GPI) and the mCherry–VAMP2 or mCherry–VAMP8 was observed using an Olympus FV1000D laser-scanning microscope (Olympus) with UPLSAPO 60× and 100× objective lenses (NA 1.35 and 1.40, respectively; Olympus).

IUE

The following sgRNA target sequences used to knockout SNAP23, VAMP8, Stx1B, SNAP25, or Stx1A were cloned into the BbsI site of a pX330 plasmid (Addgene #42230): SNAP23: 5′-AGTTCAGCTGCGGGCTCACCAGG-3′ or 5′-GGCTCACCAGGTTACTGATGAGG-3′; VAMP8: 5′-AGTCCTCTGTCTTGTTTCGGAGG-3′; Stx1B: 5′-TAAAGTGGTCTCGATCCACGTGG-3′ or 5′-TATGGATGAGTTCTTCGAGCAGG-3′; SNAP25: 5′-CATGTCTGCGTCTTCGGCCATGG-3′; and Stx1A: 5′-CCGAACCCAGGAGCTCCGCACGG-3′ or 5′-ATTCATCCATGAAGCGGTCTCGG-3′.

IUE was performed using previously described methods (Kalebic et al., 2016; Shinmyo et al., 2016). Briefly, pregnant ICR mice were anesthetized and the uterus was exposed at E13.5. The pX330 plasmid, with or without the sgRNA target sequence, and mCherry plasmid were injected with a glass micropipette into the lateral ventricle of each embryo. For the rescue experiment, the N-cadherin–LDLR–mCherry plasmid was made by a modification of an N-cadherin–mCherry plasmid (Fig. 5 E). The N-cadherin–mCherry or N-cadherin–LDLR–mCherry plasmid was coelectroporated with SNAP23 sgRNA plasmid. For the upregulation of the Notch signaling pathway, an NICD plasmid (a gift from Dr. Raphael Kopan, University of Cincinnati, Cincinnati, Ohio; Addgene, #41730) and a 12xCSL-d1EGFP plasmid (a gift from Dr. Urban Lendahl, Karolinska Institute, Stockholm, Sweden; Addgene, #47684) were used. Electroporation was performed five times with 40-V pulses for 50 ms at 1-s intervals using a BEX CUT-21 electroporator. Embryos were fixed with 3% PFA at E15.5, and histological analyses were performed as described above.

Statistics

The data were analyzed using Excel (Microsoft) and JMP Pro 14 (SAS Institute) software. Significance was calculated using a two-tailed paired Student's *t* test. A P value of <0.05 was considered statistically significant. Data distribution was assumed to be normal, but this was not formally tested.

Online supplemental material

Fig. S1 shows immunostaining of SNAP23, VAMP8, Stx1B, Nestin, SNAP25, N-cadherin, Pals1, and Crb3 in the WT cerebral cortex. Fig. S2 shows immunoblot and cell aggregation assays and immunostaining that was performed with control RGCs and SNAP23-, VAMP3-, VAMP4-, VAMP-5-, VAMP8-, or Stx1B-depleted RGCs. Fig. S3 shows fluorescence images of SBP–EGFP–N-cadherin, mCherry–VAMP8, and SBP–mCherry–GPI 60 min after biotin treatment in the COS7 cells. Fig. S4 shows immunostaining of SNAP23, VAMP8, Stx1B, and ZO-1 in the non-electroporated region of the cerebral cortex. Fig. S5 shows immunostaining of SNAP25, Stx1A, and Par3 in the sgRNA electroporated region of the cerebral cortex. Video 1 shows the ataxic gait of a P14 NcKO mouse. Video 2 shows live-cell imaging of the intracellular trafficking of SBP–EGFP–N-cadherin and mCherry–VAMP8 in COS7 cells. Table S1 lists the SNARE proteins that coimmunoprecipitated with SNAP23, as detected by mass spectrometry.

Acknowledgments

We thank Dr. K. Moriwaki, M. Taniguchi, M. Abe, and all other members of the Harada laboratory for their kind assistance and helpful comments. We also thank Dr. Y. Honma, M. Kawano, T. Kagisaki, K. Minami, R. Higashiura, and Y. Tatsumi for providing technical support; Dr. F. Perez for providing the RUSH plasmid; and Dr. D. Massey-Harroche for providing the Crb3 antibody. Assistance with imaging analyses was provided by the Center for Medical Research and Education, Graduate School of Medicine, Osaka University. Assistance with the mass spectrometry analysis was provided by the Center of Medical Innovation and Translational Research, Graduate School of Medicine, Osaka University.

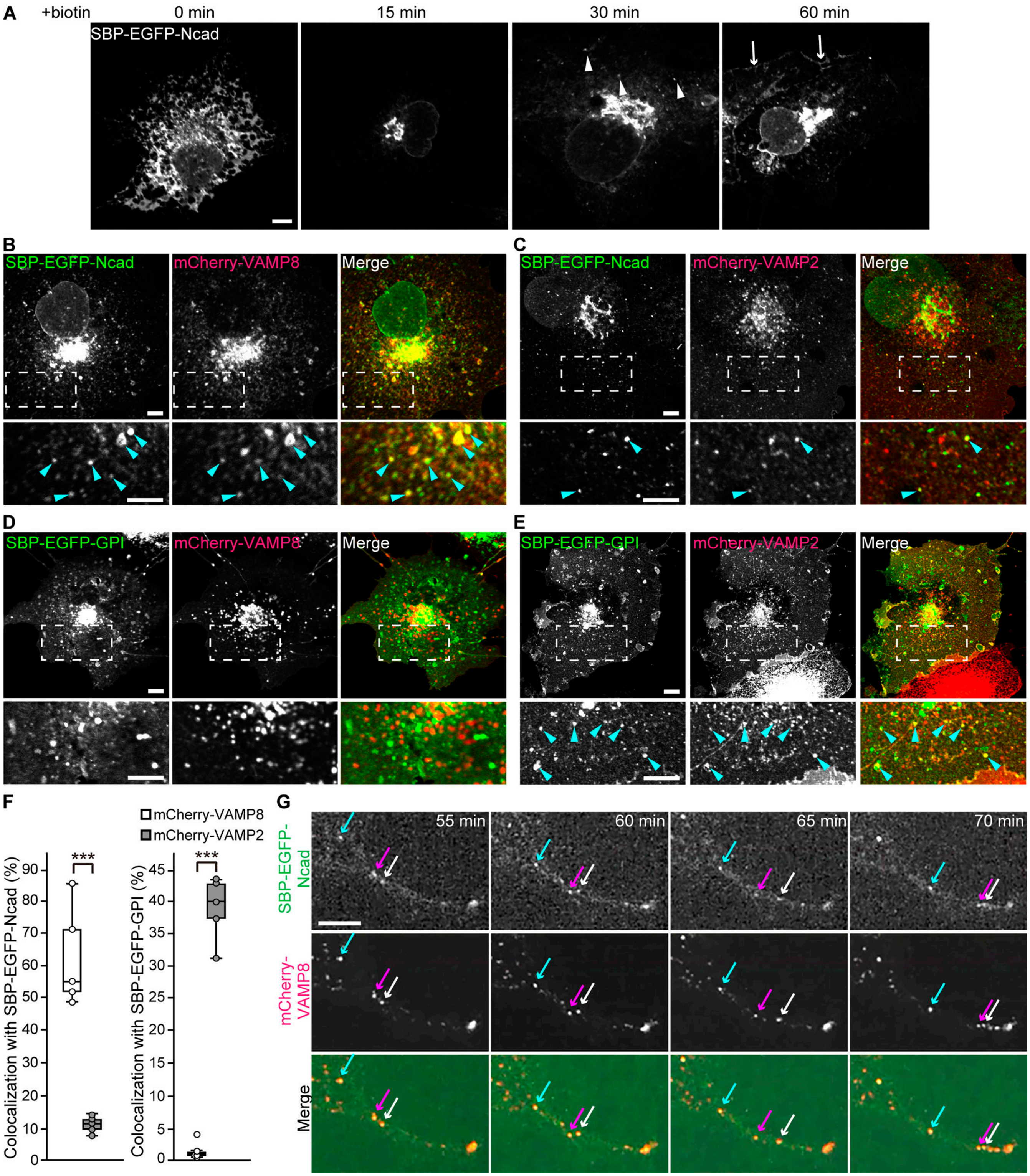
A
+biotin
0 min
15 min
30 min
60 min
SBP-EGFP-Ncad
B
SBP-EGFP-Ncad
mCherry-VAMP8
Merge
C
SBP-EGFP-Ncad
mCherry-VAMP2
Merge
D
SBP-EGFP-GPI
mCherry-VAMP8
Merge
E
SBP-EGFP-GPI
mCherry-VAMP2
Merge
F
mCherry-VAMP8
mCherry-VAMP2
***
***
Colocalization with SBP-EGFP-Ncad (%)
0
10
20
30
40
50
60
70
80
90
Colocalization with SBP-EGFP-GPI (%)
0
5
10
15
20
25
30
35
40
45
G
55 min
60 min
65 min
70 min
SBP-EGFP-Ncad
mCherry-VAMP8
Merge

Figure 9. **N-cadherin is transported by VAMP8-positive transport vesicles. (A)** Fluorescence images of SBP–EGFP–N-cadherin (Ncad) in the COS7 cells after biotin treatment. The arrowheads in the image at 30 min indicate vesicular structures transported from the Golgi to the PM. The arrows in the image at 60 min indicate PM-localized N-cadherin. Scale bar, 5 µm. **(B–E)** Fluorescence images of SBP–EGFP–Ncad (B and C) or SBP–EGFP–GPI (D and E) and mCherry–VAMP8 (B and D) or mCherry–VAMP2 (C and F) in the COS7 cells 60 min after biotin treatment. Blue arrowheads indicate EGFP and mCherry double-positive vesicular structures. Lower panels show magnified images of the boxes surrounded by dashed lines in the upper panels. Scale bars, 5 µm. **(F)** The rate of colocalization of SBP–EGFP–Ncad or SBP–EGFP–GPI and mCherry–VAMP8 or mCherry–VAMP2 (n = 5 images from each pair). **(G)** Time-lapse imaging of SBP–EGFP–Ncad and mCherry–VAMP8 after biotin treatment of the COS7 cells. The blue, red, white arrows indicate the same transported double-positive vesicular structures (see also Video 2). The box plots represent the maximum and minimum values. The centerlines of the box plots represent the medians of the data. Significance was calculated using two-tailed paired Student's *t* tests. Statistical significance is indicated by ***P < 0.001.

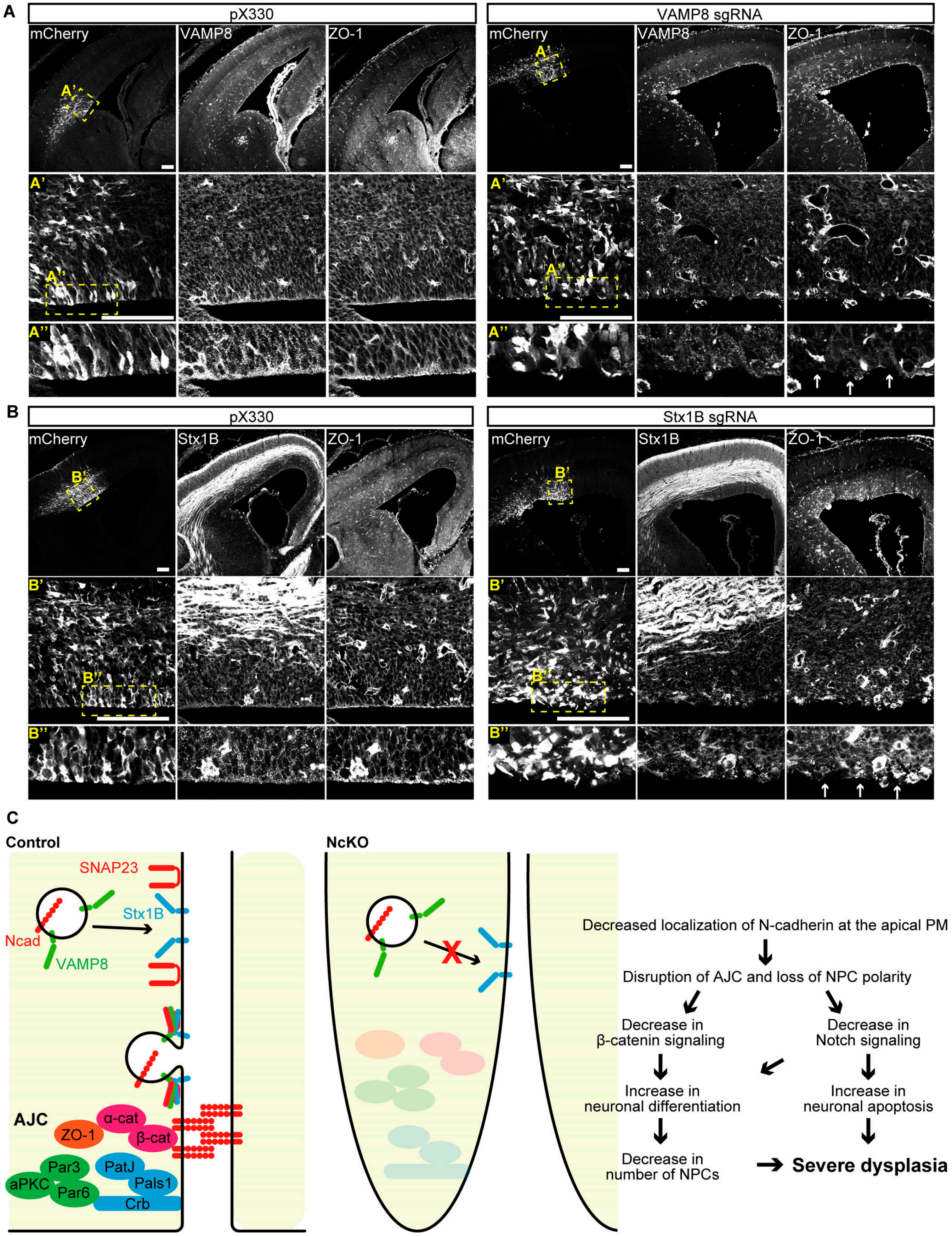
A
pX330
VAMP8 sgRNA
mCherry
VAMP8
ZO-1
A'
A''
B
pX330
Stx1B sgRNA
mCherry
Stx1B
ZO-1
B'
B''
C
Control
SNAP23
Stx1B
Ncad
VAMP8
AJC
ZO-1
α-cat
β-cat
Par3
PatJ
aPKC
Pals1
Par6
Crb
NcKO
Decreased localization of N-cadherin at the apical PM
Disruption of AJC and loss of NPC polarity
Decrease in β-catenin signaling
Decrease in Notch signaling
Increase in neuronal differentiation
Increase in neuronal apoptosis
Decrease in number of NPCs
Severe dysplasia

Figure 10. **VAMP8 or Stx1B deficiency disrupts AJCs in vivo. (A and B)** VAMP8 (A) or Stx1B (B) and ZO-1 stained in the electroporated region of the cerebral cortex. pX330 was electroporated as a control. mCherry staining shows the electroporated region. Lower panels (A′, A′′, B′, and B′′) show magnified images of the boxes surrounded by dashed lines in the upper panels. The arrows indicate the disruption of AJCs and the loss of the clear boundary of the ventricular surface. Scale bars, 100 µm. **(C)** A hypothetical model showing the cause of malformation in NcKO mice. Ncad, N-cadherin; NPC, neural progenitor cell.

This study was supported by KAKENHI grants from the Japan Society for the Promotion of Science (JP15H04668, JP17H06422, and JP18H02594 to A. Harada; and JP17K17847 to M. Kunii) and by the Joint Research Program of the Institute for Molecular and Cellular Regulation, Gunma University.

The authors declare that they have no competing interests.

Author contributions: A. Harada, M. Ogawa, and M. Kunii designed the experiments. M. Kunii performed most of the experiments and analyzed the data with assistance from Y. Noguchi. S. Yoshimura supervised the biochemical studies. S. Kanda performed the immunoblotting of the SNARE proteins. T. Iwano supervised the in utero electroporation. E. Avriyanti and N. Atik performed cell surface biotinylation assays with M. Kunii. T. Sato supervised the generation of the SNAP23 KO mice. M. Ogawa supervised the culture of the RGCs. A. Harada and K. Sato supervised the project. M. Kunii and A. Harada wrote the manuscript.

Submitted: 13 October 2019
Revised: 23 August 2020
Accepted: 23 October 2020

References

Assémat, E., E. Bazellières, E. Pallesi-Pocachard, A. Le Bivic, and D. Massey-Harroche. 2008. Polarity complex proteins. *Biochim. Biophys. Acta.* 1778: 614–630. https://doi.org/10.1016/j.bbamem.2007.08.029

Atik, N., M. Kunii, E. Avriyanti, N. Furumoto, K. Inami, S. Yoshimura, R. Harada, and A. Harada. 2014. The role of PKD in cell polarity, biosynthetic pathways, and organelle/F-actin distribution. *Cell Struct. Funct.* 39:61–77. https://doi.org/10.1247/csf.13020

Boncompain, G., S. Divoux, N. Gareil, H. de Forges, A. Lescure, L. Latreche, V. Mercanti, F. Jollivet, G. Raposo, and F. Perez. 2012. Synchronization of secretory protein traffic in populations of cells. *Nat. Methods.* 9:493–498. https://doi.org/10.1038/nmeth.1928

Bryant, D.M., and J.L. Stow. 2004. The ins and outs of E-cadherin trafficking. *Trends Cell Biol.* 14:427–434. https://doi.org/10.1016/j.tcb.2004.07.007

Bultje, R.S., D.R. Castaneda-Castellanos, L.Y. Jan, Y.N. Jan, A.R. Kriegstein, and S.H. Shi. 2009. Mammalian Par3 regulates progenitor cell asymmetric division via notch signaling in the developing neocortex. *Neuron.* 63:189–202. https://doi.org/10.1016/j.neuron.2009.07.004

Burden, J.J., X.M. Sun, A.B.G. García, and A.K. Soutar. 2004. Sorting motifs in the intracellular domain of the low density lipoprotein receptor interact with a novel domain of sorting nexin-17. *J. Biol. Chem.* 279:16237–16245. https://doi.org/10.1074/jbc.M313689200

Butts, T., M.J. Green, and R.J.T. Wingate. 2014. Development of the cerebellum: simple steps to make a 'little brain'. *Development.* 141:4031–4041. https://doi.org/10.1242/dev.106559

Cadwell, C.M., W. Su, and A.P. Kowalczyk. 2016. Cadherin tales: Regulation of cadherin function by endocytic membrane trafficking. *Traffic.* 17: 1262–1271. https://doi.org/10.1111/tra.12448

Chenn, A., and C.A. Walsh. 2002. Regulation of cerebral cortical size by control of cell cycle exit in neural precursors. *Science.* 297:365–369. https://doi.org/10.1126/science.1074192

Chenn, A., Y.A. Zhang, B.T. Chang, and S.K. McConnell. 1998. Intrinsic polarity of mammalian neuroepithelial cells. *Mol. Cell. Neurosci.* 11:183–193. https://doi.org/10.1006/mcne.1998.0680

Dudok, J.J., M. Murtaza, C. Henrique Alves, P. Rashbass, and J. Wijnholds. 2016. Crumbs 2 prevents cortical abnormalities in mouse dorsal telencephalon. *Neurosci. Res.* 108:12–23. https://doi.org/10.1016/j.neures.2016.01.001

Fujiwara, T., T. Mishima, T. Kofuji, T. Chiba, K. Tanaka, A. Yamamoto, and K. Akagawa. 2006. Analysis of knock-out mice to determine the role of HPC-1/syntaxin 1A in expressing synaptic plasticity. *J. Neurosci.* 26: 5767–5776. https://doi.org/10.1523/JNEUROSCI.0289-06.2006

Götz, M., and W.B. Huttner. 2005. The cell biology of neurogenesis. *Nat. Rev. Mol. Cell Biol.* 6:777–788. https://doi.org/10.1038/nrm1739

Graus-Porta, D., S. Blaess, M. Senften, A. Littlewood-Evans, C. Damsky, Z. Huang, P. Orban, R. Klein, J.C. Schittny, and U. Müller. 2001. Beta1-class integrins regulate the development of laminae and folia in the cerebral and cerebellar cortex. *Neuron.* 31:367–379. https://doi.org/10.1016/S0896-6273(01)00374-9

Gumbiner, B.M. 2005. Regulation of cadherin-mediated adhesion in morphogenesis. *Nat. Rev. Mol. Cell Biol.* 6:622–634. https://doi.org/10.1038/nrm1699

Gupta, A., L.H. Tsai, and A. Wynshaw-Boris. 2002. Life is a journey: a genetic look at neocortical development. *Nat. Rev. Genet.* 3:342–355. https://doi.org/10.1038/nrg799

Hong, W. 2005. SNAREs and traffic. *Biochim. Biophys. Acta.* 1744:120–144. https://doi.org/10.1016/j.bbamcr.2005.03.014

Imai, F., S. Hirai, K. Akimoto, H. Koyama, T. Miyata, M. Ogawa, S. Noguchi, T. Sasaoka, T. Noda, and S. Ohno. 2006. Inactivation of aPKCλ results in the loss of adherens junctions in neuroepithelial cells without affecting neurogenesis in mouse neocortex. *Development.* 133:1735–1744. https://doi.org/10.1242/dev.02330

Itakura, E., C. Kishi-Itakura, and N. Mizushima. 2012. The hairpin-type tail-anchored SNARE syntaxin 17 targets to autophagosomes for fusion with endosomes/lysosomes. *Cell.* 151:1256–1269. https://doi.org/10.1016/j.cell.2012.11.001

Jahn, R., and R.H. Scheller. 2006. SNAREs--engines for membrane fusion. *Nat. Rev. Mol. Cell Biol.* 7:631–643. https://doi.org/10.1038/nrm2002

Jossin, Y., M. Lee, O. Klezovitch, E. Kon, A. Cossard, W.H. Lien, T.E. Fernandez, J.A. Cooper, and V. Vasioukhin. 2017. Llgl1 Connects Cell Polarity with Cell-Cell Adhesion in Embryonic Neural Stem Cells. *Dev. Cell.* 41:481–495.e5. https://doi.org/10.1016/j.devcel.2017.05.002

Kádková, A., J. Radecke, and J.B. Sørensen. 2019. The SNAP-25 Protein Family. *Neuroscience.* 420:50–71. https://doi.org/10.1016/j.neuroscience.2018.09.020

Kadowaki, M., S. Nakamura, O. Machon, S. Krauss, G.L. Radice, and M. Takeichi. 2007. N-cadherin mediates cortical organization in the mouse brain. *Dev. Biol.* 304:22–33. https://doi.org/10.1016/j.ydbio.2006.12.014

Kalebic, N., E. Taverna, S. Tavano, F.K. Wong, D. Suchold, S. Winkler, W.B. Huttner, and M. Sarov. 2016. CRISPR/Cas9-induced disruption of gene expression in mouse embryonic brain and single neural stem cells in vivo. *EMBO Rep.* 17:338–348. https://doi.org/10.15252/embr.201541715

Kim, S., M.K. Lehtinen, A. Sessa, M.W. Zappaterra, S.H. Cho, D. Gonzalez, B. Boggan, C.A. Austin, J. Wijnholds, M.J. Gambello, et al. 2010. The apical complex couples cell fate and cell survival to cerebral cortical development. *Neuron.* 66:69–84. https://doi.org/10.1016/j.neuron.2010.03.019

Kunii, M., M. Ohara-Imaizumi, N. Takahashi, M. Kobayashi, R. Kawakami, Y. Kondoh, T. Shimizu, S. Simizu, B. Lin, K. Nunomura, et al. 2016. Opposing roles for SNAP23 in secretion in exocrine and endocrine pancreatic cells. *J. Cell Biol.* 215:121–138. https://doi.org/10.1083/jcb.201604030

Lehtinen, M.K., and C.A. Walsh. 2011. Neurogenesis at the brain-cerebrospinal fluid interface. *Annu. Rev. Cell Dev. Biol.* 27:653–679. https://doi.org/10.1146/annurev-cellbio-092910-154026

Machon, O., C.J. van den Bout, M. Backman, R. Kemler, and S. Krauss. 2003. Role of beta-catenin in the developing cortical and hippocampal neuroepithelium. *Neuroscience.* 122:129–143. https://doi.org/10.1016/S0306-4522(03)00519-0

Mason, H.A., S.M. Rakowiecki, T. Gridley, and G. Fishell. 2006. Loss of notch activity in the developing central nervous system leads to increased cell death. *Dev. Neurosci.* 28:49–57. https://doi.org/10.1159/000090752

Matter, K., W. Hunziker, and I. Mellman. 1992. Basolateral sorting of LDL receptor in MDCK cells: the cytoplasmic domain contains two tyrosine-dependent targeting determinants. *Cell.* 71:741–753. https://doi.org/10.1016/0092-8674(92)90551-M

McAllister, J.P., M.M. Guerra, L.C. Ruiz, A.J. Jimenez, D. Dominguez-Pinos, D. Sival, W. den Dunnen, D.M. Morales, R.E. Schmidt, E.M. Rodriguez, and D.D. Limbrick. 2017. Ventricular Zone Disruption in Human Neonates With Intraventricular Hemorrhage. *J. Neuropathol. Exp. Neurol.* 76: 358–375. https://doi.org/10.1093/jnen/nlx017

Mellman, I., and W.J. Nelson. 2008. Coordinated protein sorting, targeting and distribution in polarized cells. *Nat. Rev. Mol. Cell Biol.* 9:833–845. https://doi.org/10.1038/nrm2525

Miranda, K.C., T. Khromykh, P. Christy, T.L. Le, C.J. Gottardi, A.S. Yap, J.L. Stow, and R.D. Teasdale. 2001. A dileucine motif targets E-cadherin to the basolateral cell surface in Madin-Darby canine kidney and LLC-PK1 epithelial cells. *J. Biol. Chem.* 276:22565–22572. https://doi.org/10.1074/jbc.M101907200

Mishima, T., T. Fujiwara, M. Sanada, T. Kofuji, M. Kanai-Azuma, and K. Akagawa. 2014. Syntaxin 1B, but not syntaxin 1A, is necessary for the regulation of synaptic vesicle exocytosis and of the readily releasable pool at central synapses. *PLoS One.* 9:e90004. https://doi.org/10.1371/journal.pone.0090004

Miyamoto, Y., F. Sakane, and K. Hashimoto. 2015. N-cadherin-based adherens junction regulates the maintenance, proliferation, and differentiation of neural progenitor cells during development. *Cell Adhes. Migr.* 9: 183–192. https://doi.org/10.1080/19336918.2015.1005466

Miyata, T., A. Kawaguchi, H. Okano, and M. Ogawa. 2001. Asymmetric inheritance of radial glial fibers by cortical neurons. *Neuron.* 31:727–741. https://doi.org/10.1016/S0896-6273(01)00420-2

Miyata, T., M. Okamoto, T. Shinoda, and A. Kawaguchi. 2015. Interkinetic nuclear migration generates and opposes ventricular-zone crowding: insight into tissue mechanics. *Front. Cell. Neurosci.* 8:473. https://doi.org/10.3389/fncel.2014.00473

Nadarajah, B., and J.G. Parnavelas. 2002. Modes of neuronal migration in the developing cerebral cortex. *Nat. Rev. Neurosci.* 3:423–432. https://doi.org/10.1038/nrn845

Nechiporuk, T., T.E. Fernandez, and V. Vasioukhin. 2007. Failure of epithelial tube maintenance causes hydrocephalus and renal cysts in Dlg5-/- mice. *Dev. Cell.* 13:338–350. https://doi.org/10.1016/j.devcel.2007.07.017

Noctor, S.C., A.C. Flint, T.A. Weissman, R.S. Dammerman, and A.R. Kriegstein. 2001. Neurons derived from radial glial cells establish radial units in neocortex. *Nature.* 409:714–720. https://doi.org/10.1038/35055553

Pevsner, J., S.C. Hsu, J.E.A. Braun, N. Calakos, A.E. Ting, M.K. Bennett, and R.H. Scheller. 1994. Specificity and regulation of a synaptic vesicle docking complex. *Neuron.* 13:353–361. https://doi.org/10.1016/0896-6273(94)90352-2

Qiu, R., X. Wang, A. Davy, C. Wu, K. Murai, H. Zhang, J.G. Flanagan, P. Soriano, and Q. Lu. 2008. Regulation of neural progenitor cell state by ephrin-B. *J. Cell Biol.* 181:973–983. https://doi.org/10.1083/jcb.200708091

Rasin, M.R., V.R. Gazula, J.J. Breunig, K.Y. Kwan, M.B. Johnson, S. Liu-Chen, H.S. Li, L.Y. Jan, Y.N. Jan, P. Rakic, and N. Sestan. 2007. Numb and Numbl are required for maintenance of cadherin-based adhesion and polarity of neural progenitors. *Nat. Neurosci.* 10:819–827. https://doi.org/10.1038/nn1924

Ravichandran, V., A. Chawla, and P.A. Roche. 1996. Identification of a novel syntaxin- and synaptobrevin/VAMP-binding protein, SNAP-23, expressed in non-neuronal tissues. *J. Biol. Chem.* 271:13300–13303. https://doi.org/10.1074/jbc.271.23.13300

Ren, B., Z. Azzegagh, A.M. Jaramillo, Y. Zhu, A. Pardo-Saganta, R. Bagirzadeh, J.R. Flores, W. Han, Y.J. Tang, J. Tu, et al. 2015. SNAP23 is selectively expressed in airway secretory cells and mediates baseline and stimulated mucin secretion. *Biosci. Rep.* 35:e00220. https://doi.org/10.1042/BSR20150004

Rodríguez, E.M., M.M. Guerra, K. Vío, C. González, A. Ortloff, L.F. Bátiz, S. Rodríguez, M.C. Jara, R.I. Muñoz, E. Ortega, et al. 2012. A cell junction pathology of neural stem cells leads to abnormal neurogenesis and hydrocephalus. *Biol. Res.* 45:231–242. https://doi.org/10.4067/S0716-97602012000300005

Sakakibara, S., T. Imai, K. Hamaguchi, M. Okabe, J. Aruga, K. Nakajima, D. Yasutomi, T. Nagata, Y. Kurihara, S. Uesugi, et al. 1996. Mouse-Musashi-1, a neural RNA-binding protein highly enriched in the mammalian CNS stem cell. *Dev. Biol.* 176:230–242. https://doi.org/10.1006/dbio.1996.0130

Schoch, S., F. Deák, A. Königstorfer, M. Mozhayeva, Y. Sara, T.C. Südhof, and E.T. Kavalali. 2001. SNARE function analyzed in synaptobrevin/VAMP knockout mice. *Science.* 294:1117–1122. https://doi.org/10.1126/science.1064335

Shinmyo, Y., S. Tanaka, S. Tsunoda, K. Hosomichi, A. Tajima, and H. Kawasaki. 2016. CRISPR/Cas9-mediated gene knockout in the mouse brain using in utero electroporation. *Sci. Rep.* 6:20611. https://doi.org/10.1038/srep20611

Singh, S., and D.J. Solecki. 2015. Polarity transitions during neurogenesis and germinal zone exit in the developing central nervous system. *Front. Cell. Neurosci.* 9:62. https://doi.org/10.3389/fncel.2015.00062

Südhof, T.C., and J.E. Rothman. 2009. Membrane fusion: grappling with SNARE and SM proteins. *Science.* 323:474–477. https://doi.org/10.1126/science.1161748

Suh, Y.H., A. Terashima, R.S. Petralia, R.J. Wenthold, J.T.R. Isaac, K.W. Roche, and P.A. Roche. 2010. A neuronal role for SNAP-23 in postsynaptic glutamate receptor trafficking. *Nat. Neurosci.* 13:338–343. https://doi.org/10.1038/nn.2488

Sutton, R.B., D. Fasshauer, R. Jahn, and A.T. Brunger. 1998. Crystal structure of a SNARE complex involved in synaptic exocytosis at 2.4 A resolution. *Nature.* 395:347–353. https://doi.org/10.1038/26412

Taverna, E., M. Götz, and W.B. Huttner. 2014. The cell biology of neurogenesis: toward an understanding of the development and evolution of the neocortex. *Annu. Rev. Cell Dev. Biol.* 30:465–502. https://doi.org/10.1146/annurev-cellbio-101011-155801

Thoreson, M.A., P.Z. Anastasiadis, J.M. Daniel, R.C. Ireton, M.J. Wheelock, K.R. Johnson, D.K. Hummingbird, and A.B. Reynolds. 2000. Selective uncoupling of p120(ctn) from E-cadherin disrupts strong adhesion. *J. Cell Biol.* 148:189–202. https://doi.org/10.1083/jcb.148.1.189

Tronche, F., C. Kellendonk, O. Kretz, P. Gass, K. Anlag, P.C. Orban, R. Bock, R. Klein, and G. Schütz. 1999. Disruption of the glucocorticoid receptor gene in the nervous system results in reduced anxiety. *Nat. Genet.* 23: 99–103. https://doi.org/10.1038/12703

Uzquiano, A., I. Gladwyn-Ng, L. Nguyen, O. Reiner, M. Götz, F. Matsuzaki, and F. Francis. 2018. Cortical progenitor biology: key features mediating proliferation versus differentiation. *J. Neurochem.* 146:500–525. https://doi.org/10.1111/jnc.14338

Vardar, G., S. Chang, M. Arancillo, Y.J. Wu, T. Trimbuch, and C. Rosenmund. 2016. Distinct Functions of Syntaxin-1 in Neuronal Maintenance, Synaptic Vesicle Docking, and Fusion in Mouse Neurons. *J. Neurosci.* 36: 7911–7924. https://doi.org/10.1523/JNEUROSCI.1314-16.2016

Wang, C.C., C.P. Ng, L. Lu, V. Atlashkin, W. Zhang, L.F. Seet, and W. Hong. 2004. A role of VAMP8/endobrevin in regulated exocytosis of pancreatic acinar cells. *Dev. Cell.* 7:359–371. https://doi.org/10.1016/j.devcel.2004.08.002

Wang, C.C., H. Shi, K. Guo, C.P. Ng, J. Li, B.Q. Gan, H. Chien Liew, J. Leinonen, H. Rajaniemi, Z.H. Zhou, et al. 2007. VAMP8/endobrevin as a general vesicular SNARE for regulated exocytosis of the exocrine system. *Mol. Biol. Cell.* 18:1056–1063. https://doi.org/10.1091/mbc.e06-10-0974

Washbourne, P., P.M. Thompson, M. Carta, E.T. Costa, J.R. Mathews, G. Lopez-Benditó, Z. Molnár, M.W. Becher, C.F. Valenzuela, L.D. Partridge, and M.C. Wilson. 2002. Genetic ablation of the t-SNARE SNAP-25 distinguishes mechanisms of neuroexocytosis. *Nat. Neurosci.* 5:19–26. https://doi.org/10.1038/nn783

Weisz, O.A., and E. Rodriguez-Boulan. 2009. Apical trafficking in epithelial cells: signals, clusters and motors. *J. Cell Sci.* 122:4253–4266. https://doi.org/10.1242/jcs.032615

Wu, Y.J., R. Tejero, M. Arancillo, G. Vardar, T. Korotkova, M. Kintscher, D. Schmitz, A. Ponomarenko, L. Tabares, and C. Rosenmund. 2015. Syntaxin 1B is important for mouse postnatal survival and proper synaptic function at the mouse neuromuscular junctions. *J. Neurophysiol.* 114: 2404–2417. https://doi.org/10.1152/jn.00577.2015

Zechner, D., Y. Fujita, J. Hülsken, T. Müller, I. Walther, M.M. Taketo, E.B. Crenshaw III, W. Birchmeier, and C. Birchmeier. 2003. beta-Catenin signals regulate cell growth and the balance between progenitor cell expansion and differentiation in the nervous system. *Dev. Biol.* 258: 406–418. https://doi.org/10.1016/S0012-1606(03)00123-4

Supplemental material

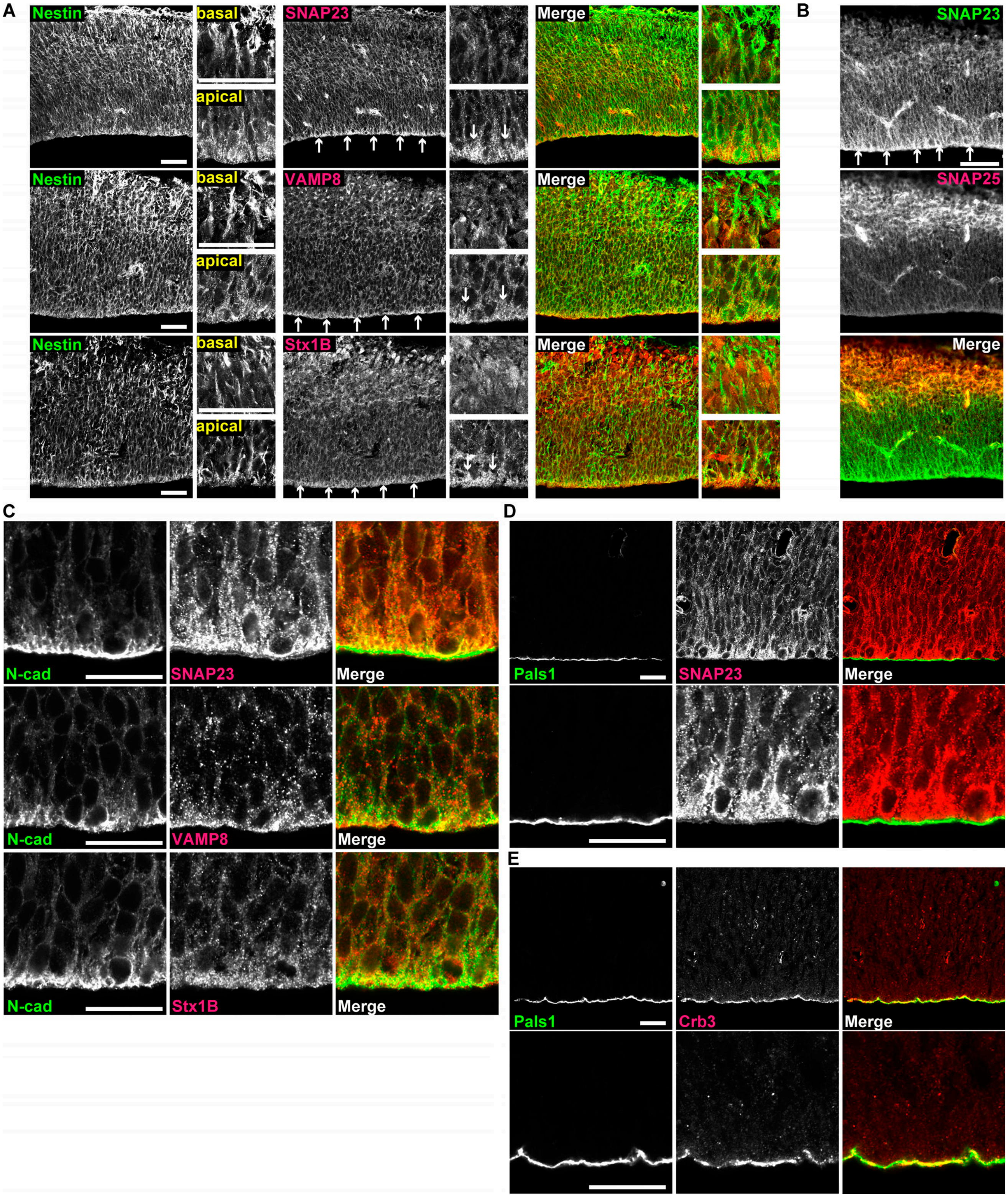
A
Nestin
basal
apical
SNAP23
Merge
B
SNAP23
Nestin
basal
apical
VAMP8
Merge
SNAP25
Nestin
basal
apical
Stx1B
Merge
Merge
C
D
N-cad
SNAP23
Merge
Pals1
SNAP23
Merge
N-cad
VAMP8
Merge
E
N-cad
Stx1B
Merge
Pals1
Crb3
Merge

Figure S1. **Localization of SNAP23, VAMP8, and Stx1B in the cerebral cortex of WT mice at E13.5. (A)** Nestin (green) and SNAP23 (upper, red), VAMP8 (middle, red), or Stx1B (lower, red) stained in the cerebral cortex of the WT mice at E13.5. Arrows indicate the apical side of the RGCs. Scale bars, 50 µm. **(B)** SNAP23 (green) and SNAP25 (red) stained in the cerebral cortex of the WT mice at E13.5. SNAP23 preferentially localizes to the apical side of the RGCs (arrows), whereas SNAP25 localizes to the pial side. Scale bar, 50 µm. **(C)** N-cadherin (N-cad; green) and SNAP23 (upper, red), VAMP8 (middle, red), or Stx1B (lower, red) stained in the cerebral cortex of the WT mice at E13.5. Scale bars, 20 µm. These SNARE components and N-cadherin are partially colocalized to the apical side in RGCs. **(D)** Pals1 (green) and SNAP23 (red) stained in the cerebral cortex of the WT mice at E13.5. Scale bars, 20 µm. More Pals1 than SNAP23 localize to the apical side of the RGCs. **(E)** Pals1 (green) and Crb3 (red) stained in the cerebral cortex of the WT mice at E13.5. Scale bars, 20 µm. Crb3 and Pals1 are colocalized at the apical surface of the RGCs.

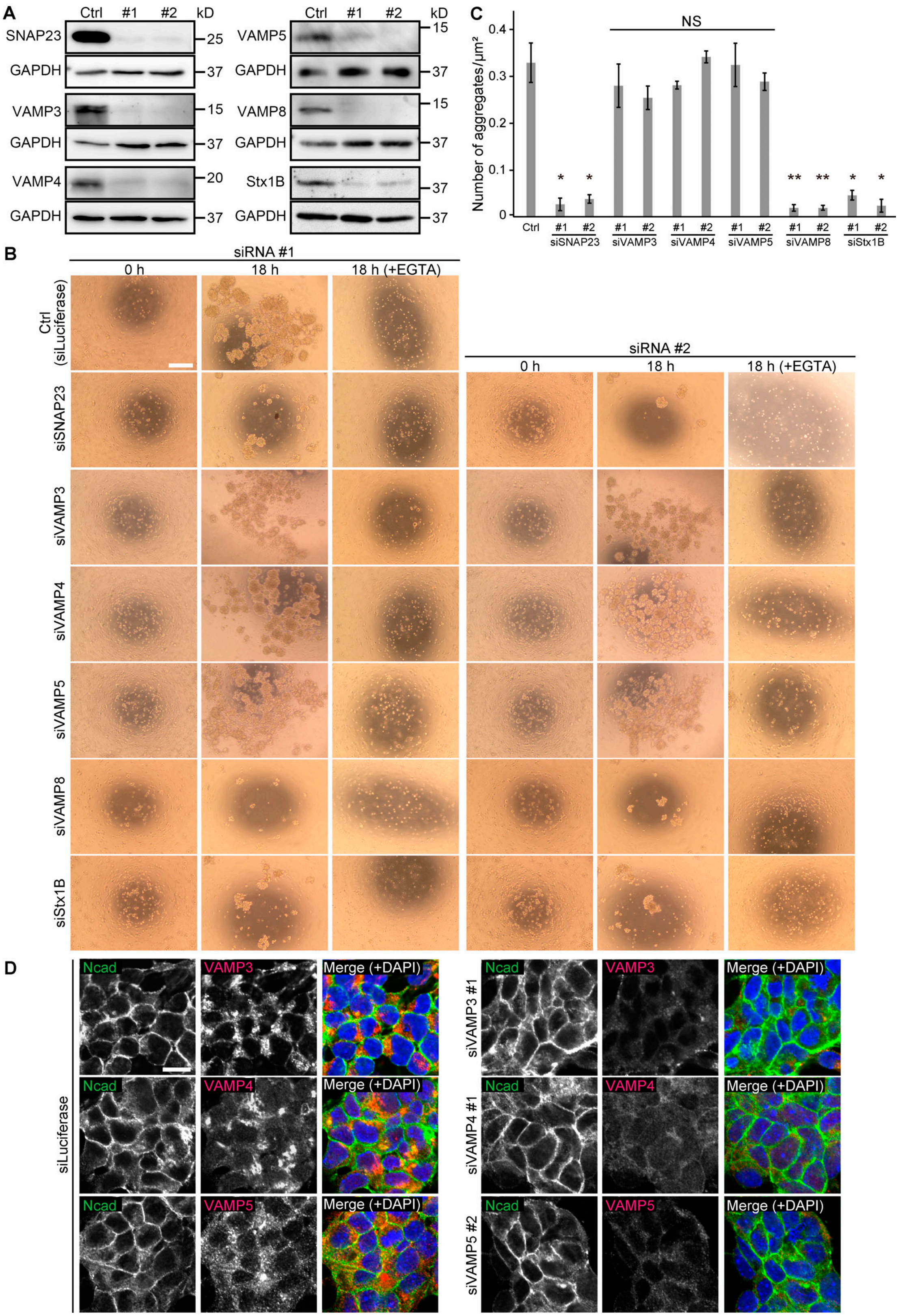
A
Ctrl
#1
#2
kD
SNAP23
25
GAPDH
37
VAMP3
15
GAPDH
37
VAMP4
20
GAPDH
37
VAMP5
15
GAPDH
37
VAMP8
15
GAPDH
37
Stx1B
37
GAPDH
37
C
NS
Number of aggregates/µm²
0.4
0.3
0.2
0.1
0
*
*
**
**
*
*
Ctrl
#1
#2
siSNAP23
siVAMP3
siVAMP4
siVAMP5
siVAMP8
siStx1B
B
siRNA #1
0 h
18 h
18 h (+EGTA)
siRNA #2
Ctrl (siLuciferase)
siSNAP23
siVAMP3
siVAMP4
siVAMP5
siVAMP8
siStx1B
D
Ncad
VAMP3
Merge (+DAPI)
VAMP4
VAMP5
siLuciferase
siVAMP3 #1
siVAMP4 #1
siVAMP5 #2

Figure S2. **Knockdown of SNARE proteins in cultured RGCs. (A)** Immunoblots showing each SNARE protein in the control (Ctrl) RGCs and RGCs with each SNARE protein depleted. **(B and C)** Cell aggregation assay of control RGCs and RGCs with each SNARE protein depleted and treated with or without 5 mM EGTA. The density of the aggregates was determined based on three independent experiments (C). Scale bar, 100 µm. **(D)** N-cadherin (Ncad; green) and VAMP3 (upper, red), VAMP4 (middle, red), or VAMP5 (lower, red) stained with DAPI (blue) in the control and VAMP3-, VAMP4-, or VAMP5-depleted RGCs. Scale bar, 10 µm. The bar graph represents the means ± SEM. Significance was calculated using two-tailed paired Student's *t* tests. Statistical significance is indicated by $^{*}P < 0.05$ or $^{**}P < 0.01$.

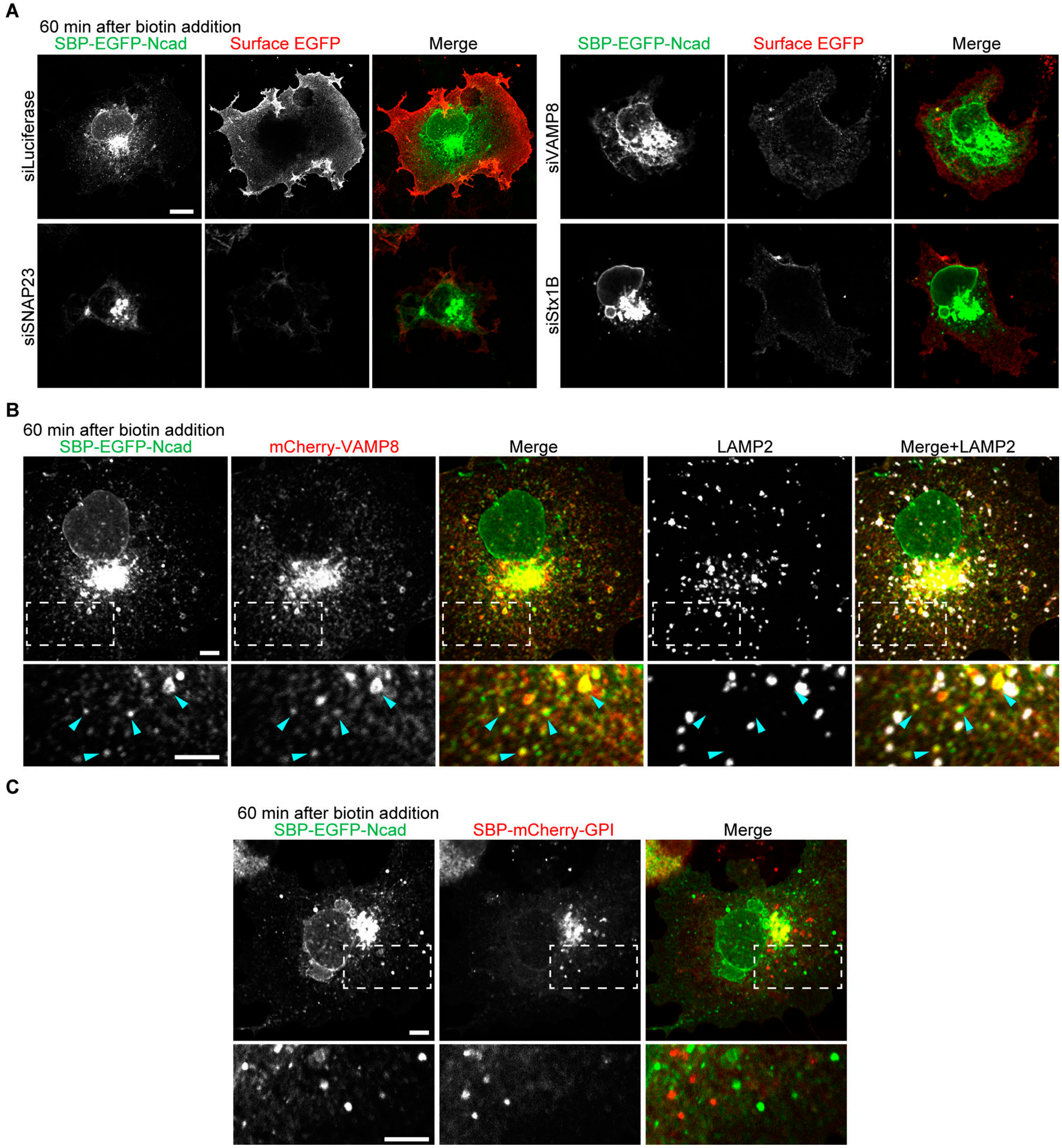
A
60 min after biotin addition
SBP-EGFP-Ncad
Surface EGFP
Merge
SBP-EGFP-Ncad
Surface EGFP
Merge
siLuciferase
siSNAP23
siVAMP8
siStx1B
B
60 min after biotin addition
SBP-EGFP-Ncad
mCherry-VAMP8
Merge
LAMP2
Merge+LAMP2
C
60 min after biotin addition
SBP-EGFP-Ncad
SBP-mCherry-GPI
Merge

Figure S3. **SBP–EGFP–N-cadherin is delivered to the PM by SNAP23, VAMP8, and Stx1B in the COS7 cells. (A)** Fluorescence images of total SBP–EGFP–N-cadherin (Ncad; green) and cell surface SBP–EGFP–Ncad labeled by GFP antibody (red) in the control (siLuciferase) and SNAP23-, VAMP8-, or Stx1B-depleted COS7 cells 60 min after biotin treatment. The cells were stained under nonpermeabilized conditions. Scale bars, 5 µm. **(B)** Fluorescence images of SBP–EGFP–Ncad, mCherry–VAMP8, and LAMP2 (a lysosome marker) in the COS7 cells 60 min after biotin treatment. The depicted cell is the same cell shown in Fig. 9 B. EGFP and mCherry double-positive vesicular structures (blue arrowheads) are not colocalized with LAMP2 (white puncta in the right panels). Lower panels show magnified images of the boxes surrounded by dashed lines in the upper panels. Scale bars, 5 µm. **(C)** Fluorescence images of SBP–EGFP–Ncad and SBP–mCherry–GPI in the COS7 cells 60 min after biotin treatment. Lower panels show magnified images of the boxes surrounded by dashed lines in the upper panels. Scale bars, 5 µm.

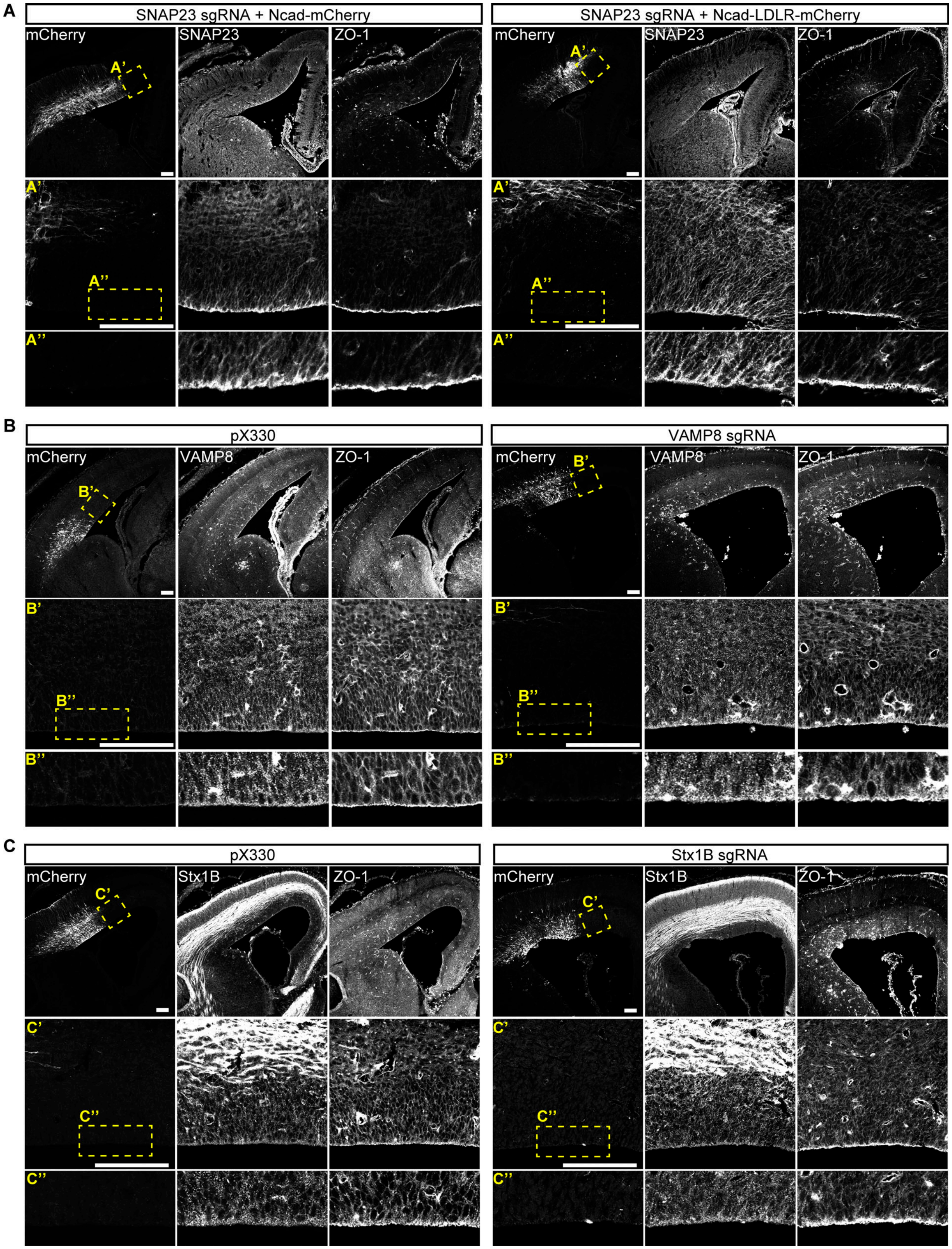
A
SNAP23 sgRNA + Ncad-mCherry
mCherry
SNAP23
ZO-1
A'
A''
SNAP23 sgRNA + Ncad-LDLR-mCherry
mCherry
SNAP23
ZO-1
A'
A''
B
pX330
mCherry
VAMP8
ZO-1
B'
B''
VAMP8 sgRNA
mCherry
VAMP8
ZO-1
B'
B''
C
pX330
mCherry
Stx1B
ZO-1
C'
C''
Stx1B sgRNA
mCherry
Stx1B
ZO-1
C'
C''

Figure S4. **AJCs are intact in the nonelectroporated region. (A)** SNAP23 and ZO-1 stained in the nonelectroporated region of the cerebral cortex. The sections are the same sections shown in Fig. 5 F (right) and Fig. 5 G (right). mCherry staining shows the electroporated region. The lower panels (A′ and A′′) show magnified images of the boxes surrounded by dashed lines in the upper panels. Scale bars, 100 µm. **(B and C)** VAMP8 (B) or Stx1B (C) and ZO-1 stained in the nonelectroporated region of the cerebral cortex. The sections are same sections shown in Fig. 10, A and B. pX330 was electroporated as a control. mCherry staining shows the electroporated region. The lower panels (B′, B′′, C′, and C′′) show magnified images of the boxes surrounded by dashed lines in the upper panels. Scale bars, 100 µm. Ncad, N-cadherin.

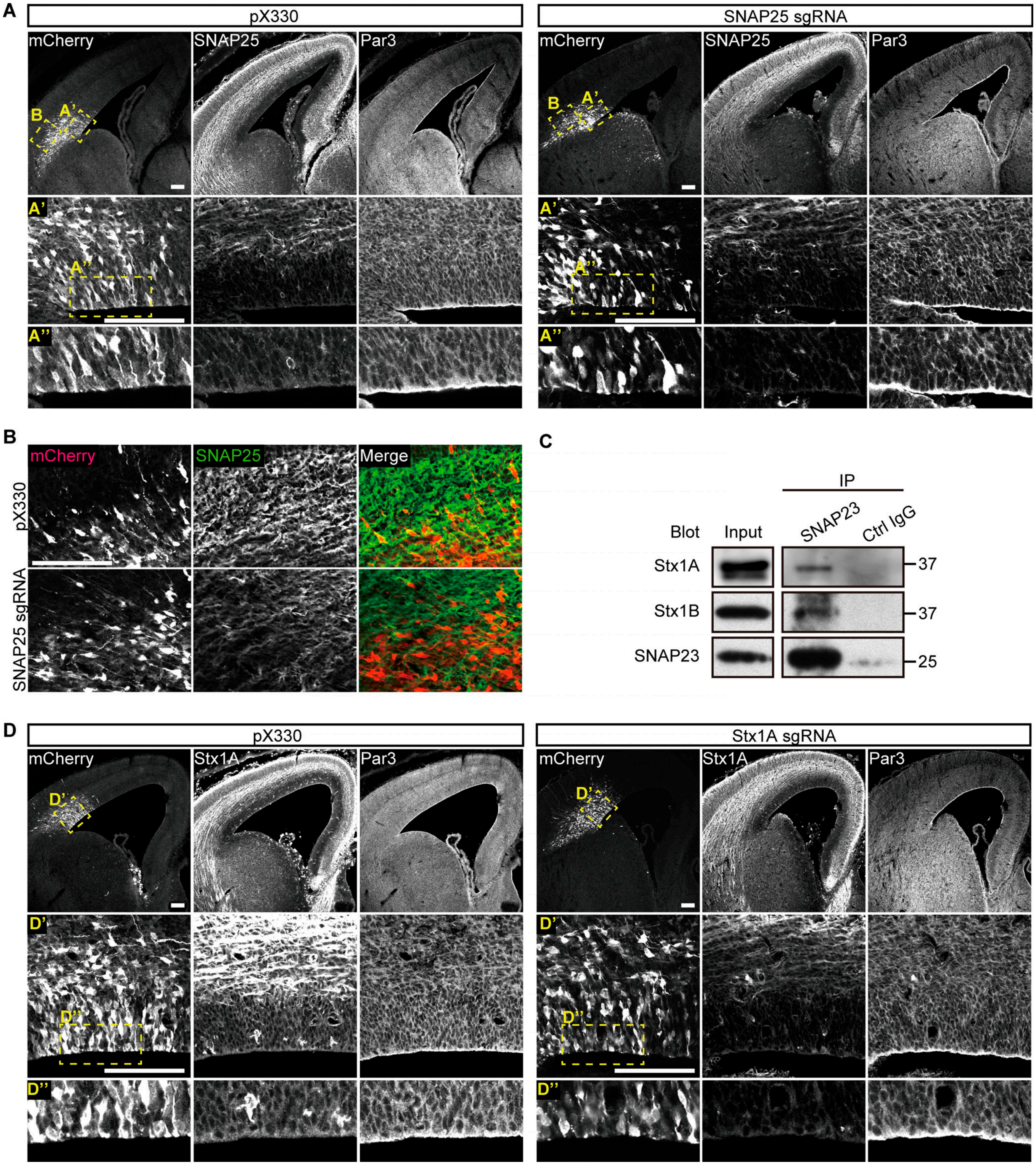
A
pX330
SNAP25 sgRNA
mCherry
SNAP25
Par3
B
A'
A''
B
pX330
SNAP25 sgRNA
mCherry
SNAP25
Merge
C
IP
Blot
Input
SNAP23
Ctrl IgG
Stx1A
Stx1B
SNAP23
37
37
25
D
pX330
Stx1A sgRNA
mCherry
Stx1A
Par3
D'
D''

Figure S5. **AJCs are intact in the SNAP25 or Stx1A sgRNA electroporated region. (A)** SNAP25 and Par3 stained in the electroporated region of the cerebral cortex. pX330 was electroporated as a control. mCherry staining shows the electroporated region. Lower panels (A′ and A′′) show magnified images of the boxes surrounded by dashed lines in the upper panels. Scale bars, 100 µm. **(B)** Magnified images of the neuronal layer in the boxes surrounded by dashed lines in the upper panel of A. SNAP25 staining was decreased in the electroporated region of the neuronal layer, indicating that Cas9 and sgRNA efficiently knocked out SNAP25. Scale bar, 100 µm. **(C)** Coimmunoprecipitation of Stx1A and Stx1B in the SNAP23 immunoprecipitates (IP) from the WT E13.5 brain lysate. **(D)** Stx1A and Par3 stained in the electroporated region of the cerebral cortex. pX330 was electroporated as a control. mCherry staining shows the electroporated region. Lower panels (D′ and D′′) show magnified images of the boxes surrounded by dashed lines in the upper panels. Scale bars, 100 µm. Ctrl, control.

Video 1. **The ataxic gait of a P14 NcKO mouse.**

Video 2. **Live-cell imaging of the intracellular trafficking of SBP–EGFP–N-cadherin and mCherry–VAMP8 in the COS7 cells.** COS7 cells were transfected with vectors carrying SBP–EGFP–N-cadherin (green) and mCherry–VAMP8 (red). The release of SBP–EGFP–N-cadherin was induced by biotin treatment. Images were captured every 10 s from 15 min to 75 min after biotin addition. The video is displayed at 30 frames/s.

Table S1, which is provided online, lists the SNARE proteins that coimmunoprecipitated with SNAP23, as detected by mass spectrometry.